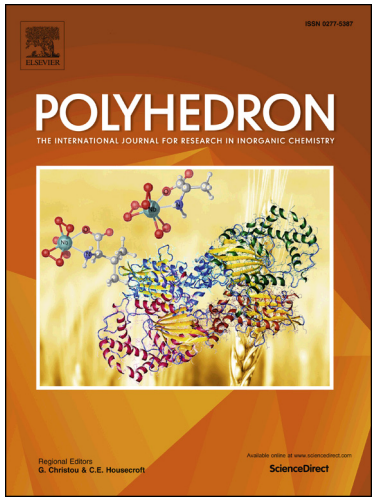

Organosuperbase dendron manganese complex grafted on magnetic nanoparticles; heterogeneous catalyst for green and selective oxidation of ethylbenzene, cyclohexene and oximes by molecular oxygen

Ali Reza Faraji, Fatemeh Ashouri, Zahra Hekmatian, Somayyeh Heydari, Sima Mosazadeh

PII: S0277-5387(18)30582-5
DOI: https://doi.org/10.1016/j.poly.2018.09.030
Reference: POLY 13429

To appear in: *Polyhedron*

Received Date: 26 April 2018
Accepted Date: 15 September 2018

Please cite this article as: A.R. Faraji, F. Ashouri, Z. Hekmatian, S. Heydari, S. Mosazadeh, Organosuperbase dendron manganese complex grafted on magnetic nanoparticles; heterogeneous catalyst for green and selective oxidation of ethylbenzene, cyclohexene and oximes by molecular oxygen, *Polyhedron* (2018), doi: https://doi.org/10.1016/j.poly.2018.09.030

Organosuperbase dendron manganese complex grafted on magnetic nanoparticles; heterogeneous catalyst for green and selective oxidation of ethylbenzene, cyclohexene and oximes by molecular oxygen

Ali Reza Faraji*[,a,b], Fatemeh Ashouri[a], Zahra Hekmatian[c], Somayyeh Heydari[d] and Sima Mosazadeh[e]

[a]*Department of Applied Chemistry, Faculty of Pharmaceutical Chemistry, Pharmaceutical Sciences Branch, Islamic Azad University, Tehran, Iran (IAUPS).*
[b]*Young Researchers and Elite Club, Pharmaceutical Sciences Branch, Islamic Azad University, Tehran, Iran (IAUPS).*
[c]*Department of Chemistry, Faculty of Science, Payam Noor University, Hamedan, Iran.*
[d]*Faculty of Chemistry, Bu-Ali-Sina University, P.O. box 651783868, Hamedan, Iran.*
[e]*Active Pharmaceutical Ingredients Research Center, Pharmaceutical Sciences Branch, Islamic Azad University, Tehran, Iran (IAUPS).*
Corresponding author. Tel.: +98 21 22640051; fax: +98 21 22600099.

E-mail address: a.faraji@iaups.ac.ir

Abstract

Magnetic Fe_3O_4 nanoparticles as a support were modified with an amino-terminated organosilicon and cyanoric choloride ligands. The novel manganese complex was grafted on modified magnetic support (Mn(II)-Met@)MMNPs). The nanocatalyst structure, particle size, morphology and surface properties was well characterized by elemental analysis, ICP-AES, AAS, EDS, FT-IR, SEM, TEM, DLS, VSM**,** TGA, XRD and XPS. In order to develop an effective heterogeneous nanocatalyst for eco-friendly aerobic, highly active and selective catalytic reactions, synthesized nanocatalyst was applied in oxidation of various organic compounds. The catalytic performance of the manganese nanocatalyst in the aerobic oxidation of ethylbenzene (EB), cyclohexene (CYHE) and various aldoximes and ketoxime were studied. Selective aerobic oxidation of EB and CYHE and various oximes were catalyzed by the Mn-nanocatalyst using N-hydroxyphthalimide (NHPI) with molecular oxygen as the green oxidant without the need of any reducing agent, and respectively the acetophenone (AcPO) as a benzylic product, 2-cyclohexene-1-one (CYHE=O) as an allylic product and corresponding carbonyl compounds were obtained. The oxidation process has been optimized for Mn-nanocatalyst by considering the effect of different parameters such as the ratio and amount of Mn-nanocatalyst/NHPI, reaction time and solvent for achieving maximum conversion and selectivity to products. Due to their significant low cost, informal preparation, easy magnetically separation

from reaction mixture, excellent catalytic performance, simple recovery and reusability without any metal leaching, the Mn-nanocatalyst has huge application prospect in selective and green oxidation process.

Keywords: Magnetic support, Manganese complex, Heterogeneous catalyst, Selective aerobic oxidation, Allylic oxidation, Benzylic oxidation.

1. Introduction

Catalytic processes are crucial for producing the new scientific foundation to making cleaner, better efficient and economically products by transformation process of crude and cheap raw material into usable and chemical industrial materials. The homogenous catalysts possess high reactivity and selectivity, because every single catalytic entity can act as a single active site. Despite in unique properties, a large number of homogenous catalytic processes reported which have not been commercialized. The difficulty manner for separation and recovery of homogenous catalyst, corrosion and deposition on reactor wall, prevent from industrialization. These disadvantages will be minimized if homogeneous complexes grafted on the nano-insoluble solid material such as SBA15, MCM, SiO_2, SiO_2/Al_2O_3 and magnetic support [1-5]. Therefore, nanostructure materials have been applied for development of heterogeneous catalysis with high selectivity and tunable control reaction conditions.

The heterogeneous nanocatalyst for green chemistry process in chemical synthesis and industry is receiving significant attention in recent periods, owing to the growing environmental concerns and depletion of green chemistry. Among various insoluble nano-materials in the field of heterogeneous catalysis, the magnetic nanoparticles have attracted increased interest due to their large adsorption capacity, excellent thermal stability, efficient recycling, low toxicity, reduced environmental impact, good thermal and chemical stabilities, low manufacture price and lower volatility being employed in a variety of chemical industries [6-8]. In addition, the large surface area and easily supporting of various ligands to the surface of Fe_3O_4 magnetic nanoparticles and easily synthesis of their metal complexes, make these nanoparticles excellent candidate for application as parent support for the development of highly active and easily reusable immobilized catalysts [9-11]. As an example, Fe_3O_4 nanoparticles supported by mesopores SBA-15 for selective removal of Ce(III) from aqueous solution [12], $Fe_3O_4@SiO_2(CH_2)_3NHArN(CH_2PPh_2)_2$ and $Fe_3O_4@SiO_2(CH_2)_3N(CH_2PPh_2)_2$ type bis(diphenylphosphinomethyl)amino ligands and their Pd(II) complexes as highly efficient

heterogeneous catalysts in conversion of 2-methyl naphthalene to 2-methyl-1,4-naphthoquinone [13], β-cyclodextrin grafted on poly(isophthalamide)/magnetic nanoparticles for the physically removing of both Gram-positive and Gram-negative bacteria [14].

One of valuable applications of above mentioned heterogeneous catalytic systems is oxidation of compounds which constitutes an important role in synthetic industrial chemistry for further modifications abundant and cheapness materials into a variety of more usable commercial chemical derivatives [15-17]. For example, The AcPO as a product of the selective oxidation of C-H bonds in benzylic position at EB in a heterogeneous catalytic process, is applied in chemical industries such as a flavoring agent in foods, the production of pharmaceuticals, fragrance in soaps and perfumes, and as a solvent for plastics and resins. Also CYHE=O previously synthesized from phenol by Birch reduction in chemical industries at harsh conditions in the presence of heterogeneous catalysts, can be prepare at mild condition reaction for using in the synthesis of a variety of chemical products such as pharmaceuticals and fragrances [18-22].

The oxidant has main role at efficiency of these catalytic systems. So, using molecular oxygen as an oxidant is more desirable from eco-friendly and green chemistry approach. For example, Aerobic oxidation of amines to imines [23, 24], green oxidation of silanes [25], aerobic oxidation of alcohols [26], aerobic oxidation of benzyl alcohol [27], aerobic oxidation of cumene [28] and selective oxidation of ethylbenzene, cyclohexene and oximes under aerobic condition [15].

Therefore, developing of simple catalytic systems with high efficiency for the aerobic oxidation of organic compounds under mild conditions is necessary. Herein, follow our previous studdies [9, 15, 17] at effective nanocatalyst, we report the immobilized manganese-metformin complex on Fe_3O_4 modified magnetic nanoparticles (Mn(II)-Met@)MMNPs) as an active recyclable heterogeneous catalyst for green oxidation of organic compounds. The efficiency of this novel heterogeneous nanocatalyst over oxidation of EB, CYHE and oximes under O_2 as a green oxidant was investigated.

2. Experimental

2.1 Materials and apparatuses

All of the chemical reagents with analytical grade used as received without further drying or purification. The solvents were purified with standard methods. For elemental analysis a CHN-Rapid Heraeus elemental analyzer (Wellesley MA) was used. ICP-AES measurements for manganese content evaluation were performed using a Perkin-Elmer ICP/6500. The specific

surface areas were calculated, using the BET method by nitrogen adsorption/desorption at 76 K on a Quantachrome NOVA automated gas sorption Instruments. The samples were degassed at 393 K for 16 h prior to the adsorption experiments. The morphology of samples was examined by a transmission electron microscopy (TEM, Philips 501 microscope) with an electron microscope operating at an 80 kV voltage. The images of SEM were taken using a Tecnai F30TEM operating at 300 kV. FT-IR spectra were obtained by Shimadzu Varian 4300Fourier Transform Infrared spectrometer in KBr pellets. For recording the thermal properties of samples, a Perkin-Elmer TG-DTA 6300 instrument at a heating rate of 15 ˚C/min. X-ray photoelectron spectroscopy (XPS) measurements was performed on a PerkinElmer PHI 5000CESCA system with a base pressure of 10^{-9} Torr. Magnetization properties of samples were analyzed by a BHV-55 VSM. The crystalline structures of samples were carried out by XRD analysis on a Bruker D8 Advance diffractometer with CuKa radiation at 40 Kv and 20 miliamper. Finally, type and quantity of the resulting products from oxidation were determined by a HP 6890/5973 GC/MS instrument and analyzed by a Shimadzu GC-16A gas chromatograph (GL-16A gas chromatograph with a 5m×3mm OV-17 column, 60–220 ˚C (10 ˚C/min), Inj. 230 ˚C, Det. 240 ˚C).

2. 2 Preparation of superparamagnetic Fe_3O_4 nanoparticles

The Fe_3O_4 magnetic nanoparticles were synthesized according to the literature [29, 30]. For making nanosized magnetic support, $FeCl_3.4H_2O$ and $FeCl_2.4H_2O$ aqueous solution in HCl (2 M) was prepared (Fe^{3+}/Fe^{2+}: 2:1). The solution was mixed and deoxygenated by N_2 gas for 20 min. Then, 50 mL of ammonia solution (37%) was added dropwise under vigorous stirring which a black solid product obtained when a reaction media reached to pH=10. The final solution was stirred for 20 min at room temperature in N_2 atmosphere and then heated at 70 °C for 30 min. The resulted black magnetite powder was separated, washed with water (3×20 ml) and dried at 80 °C for 12 h to obtain Fe_3O_4 MNPs (scheme 1, stage I).

2.3 Synthesis of SiO_2@Fe_3O_4 core-shell nanoparticles

The synthesized magnetic nanospheres Fe_3O_4 in stage I (1 g), were dispersed in EtOH/H_2O (2:1). The obtained mixture was homogenized by ultrasonication for 30 min and then ammonia solution (2 mL) was added dropwise. The solution of tetraethylorthosilicate (TEOS, 8g) in EtOH (10 mL) was injected in combination. After the reaction was performed for 100 min, the products

were collected by the help of an external magnet, washed with EtOH/H_2O and dried in vacuum for 10 h to obtain the SiO_2@Fe_3O_4 core/shell (scheme 1, stage II).

2.4 Preparation of amino-functionalized core-shell nanoparticles

The amino-functionalized core-shell nanoparticles (SiO_2-APTMS@Fe_3O_4) was prepared by refluxing prepared SiO_2@Fe_3O_4 core/shell (5.2 g) with aminopropyltrimethoxy silane (APTMS) (0.0195 mol, 3.5 mL) in dry CH_2Cl_2 (100 mL) for 24 h. The solid was filtered off, washed with CH_2Cl_2/CH_3OH (1:1) and dried at 100 °C under vacuum for 8 h (scheme 1, stage III). The carbon and nitrogen amounts were determined based on elemental analysis, 7.48 and 3.56%, respectively.

2.5 Preparation of melamine-based metformin functionalized SiO_2-APTMS@Fe_3O_4

In a typical process [30], the SiO_2-APTMS@Fe_3O_4 was dispersed and stirred in a solution of N,N-diisopropylethylamine (DIPEA) 2mL, anhydrous CH_2Cl_2 and 2,4,6-trichloro-s-triazine (cyanuric chloride, CC) for 5 h under argon atmosphere at <15 °C (scheme 1, stage IV). The resultant SiO_2-APTMS/CC@Fe_3O_4 was separated and dried under vacuum. Eventually, metformin (Met, 10 mmol) and the SiO_2-APTMS/CC@Fe_3O_4 were mixed and stirred under argon atmosphere at 80 °C for 24 h. The resultant nanoparticles (scheme 1, stage V) were easily separated from reaction mixture and washed with dichloromethane, ethanol, methanol and toluene and dried under reduced pressure at 80 °C for 8 h. The modified SiO_2@Fe_3O_4 that functionalized with APTMS/CC and metformin (Met@SiO_2-APTMS/CC/@Fe_3O_4) is defined as Met@MMNPs. The C and N% were determined 10.21 and 5.12% respectively by elemental analysis.

2.6 Preparation of supported manganese nanocatalyst

Nanocatalyst containing Mn(II)-copmlex was prepared by stirring synthesized Met@MMNPs (50 mg) with $Mn(OAc)_2 \cdot 4H_2O$ (5.4 mmol), and LiCl (8.5 mmol) in EtOH (40mL) under reflux for 24 h. Then, the obtained solid powder was filtered, washed with EtOH/MeOH and dried in vacuum at 60 ˚C to form supported manganese nanocatalyst of Mn(II)-Met@MMNPs (scheme 1, stage VI).

2.7 Catalytic performance study of immobilized manganese nanocatalyst

The selective oxidation of ethylbenzene in benzylic position, cyclohexene in allylic position and oxime, were carried out in the presence of Mn(II)-Met@MMNPs with molecular oxygen. The

conversion (Con %), selectivity (Sel%), turn over number (TON) and turn over frequency (TOF) for all substrate were calculated as follows:

(Eq.1) Substrate conversion (%) = $\frac{\mathrm{Sub_{in}} - \mathrm{Sub_{out}}}{\mathrm{Sub_{in}}} \times 100\%$

(Eq.2) Product selectivity (%) = $\frac{\text{Moles of product formed}}{\text{Moles of total products}} \times 100\%$

(Eq.3) TON = $\frac{\text{Mole of product formed}}{\text{Moles of Mn in catalyst}}$

(Eq.4) TOF (h^{-1}) = $\frac{\text{Moles of product formed}}{\text{Moles of Mn in catalyst} \times \text{reaction time (h)}}$

2.7.1 General procedure for ethylbenzene and cyclohexene oxidation with molecular oxygen

For the heterogeneous oxidation of EB and CYHE, a suspension of synthesized Mn(II)-Met@MMNPs, substrate (2 mmol), NHPI (15 mol %) and solvent (5 mL) were stirred in a three necked round bottom flask equipped with condenser and gas bubbling system and placed in a temperature controlled oil bath. For achieving best conversion and selectivity, reaction condition has been optimized by various parameters. The products from the reaction mixture were characterized by GC/MS and identified through being compared with known standards.

2.7.2 General procedure for catalytic oxidation of oximes with Molecular Oxygen

The heterogeneous aerobic oxidation of oximes were done in 3-necked round-bottom flask fitted with condenser and O_2 balloon using Mn(II)-Met@MMNPs. In typical reaction catalyst (140 mg), solvent (5 mL), oxime (2 mmol) and benzaldehyde (5 mmol) were mixed under O_2 bubbling and stirred at desired temperature. At the end of the reaction, the magnetic catalyst has been separated and products have been quantified by GC and GC-Mass through being compared with authentic samples. Furthermore, the effective various parameters in catalytic oxidation reaction were examined in order to achieve highest conversion and selectivity.

2.7.3 General procedure for recyclability study of manganese nanocatalysts

The recyclability of the Mn(II)-Met@MMNPs nanocatalyst was investigated in oxidation reaction of EB, CYHE and AcPO oxime with molecular oxygen. After any reaction, the Mn nanocatalyst was easily isolated by external magnet, recovered by being washed with fresh solvent (ether, ethanol and acetone), dried at 70 °C for 4 h and reused to next aerobic oxidation reaction.

3. Results and Discussion

3.1. Catalyst characterization

The magnetically recoverable manganese-metformin nanocatalyst was synthesized by covalently immobilization method (see scheme 1) [30]. Initially the magnetic support, which is comprise of silica-coated magnetite nanoparticles (SiO_2@Fe_3O_4, Stage I, II), was prepared, followed by its functionalization using (3-aminopropyl)triethoxysilane (3-APTES) to obtain amino groups in the surface of the core/shell support (stage III). Afterward, the surface was modified by addition of the metformin ligand (Met@MMNPs stage IV). The manganese complex was grafted of on modified magnetic support (Mn(II)-Met@MMNPs, stage V) via complex formation of Mn(II) ions. The immobilized Mn(II)-metformin nanocomplex (Mn(II)-Met@MMNPs) was characterized using CHN analysis, AAS, FT-IR, ICP-AES, BET, SEM , TEM, EDS, VSM, TGA, XRD and XPS.

The elemental composition information along with the summary of the measured and calculated values for C, H and N is presented in Table 1. These data indicate that the CHN content increased with increasing the CC and immobilized Met ligand on the surface of SiO_2@Fe_3O_4 core-shell NPs as a parent support (Table 1). The loading of manganese in nanocatalyst was evaluated by ICP-AES and elemental analyses (0.95 mol%). Supplementary experiments carried out by AAS and back titration. The content of linked Met on CC was measured via back titration process which exhibit 1.05 mmol of Met per gram of nanosupport. Furthermore, the manganese content in catalyst was estimated 0.826+0.001mmol/g by AAS. These results reveal that approximately 78.7 % of organic ligand moieties have anchored on support and efficiently coordinated with manganese ions providing catalytic active sites. The results of N_2 adsorption/desorption experiments and pore size distributions for SiO_2@Fe_3O_4 and manganese nanocatalyst are presented in Table 1. The BET surface area (S_{BET}), total pore volume (V_{BJH}), and mean pore diameter (*MPD*) of SiO_2@Fe_3O_4 is 71.1 m^2/g, 0.17 cm^3/g, and 845 A°, respectively. Remarkably, after amino functionalization of SiO_2@Fe_3O_4 with, Mn-nanocatalyst possesses a S_{BET} of 24.6 m^2/g and 24.7 m^2/g, V_{BJH} of 0.05 cm^3/g, and a MPD of 254 A°. The synthesized nanocatalyst significantly shows decrease in BET surface area and pore volume in comparison to magnetic nanosupport (Table 1, entry 1and 4). These data confirmed that organometallic cross-link was occurred though the OH of tetraethylorthosilicate on nanomagnetic parent support. Therefore, the BET surface area and the mean pore diameter decrease as a result of covering the micropore in nanomagnetic parent support. Indeed this

decrease indicates the decrease in interaction between nitrogen molecules as adsorbate and the magnetic parent support surface after immobilized of organic groups.

FT-IR spectra were conducted on both the unfunctionalized and functionalized MNPs to confirm functionalization of SiO_2, CC and Met on the Fe_3O_4 NPs (Fig. 1). The basic characteristic absorption of Fe-O vibration was observed at 585 cm^{-1} but in all spectra, this bond appears approximately 629 and 646 cm^{-1} which was attributed to the presence of the symmetric and asymmetric stretching vibrations. These peaks result from splitting of the peak at 585 cm^{-1} to 629 and 646 cm^{-1} which corresponds to the Fe-O bond at Fe_3O_4 MNPs [31]. The O–H deformed vibration at 1635 cm^{-1} was observed for curves A-F. In addition, a weak adsorption band was observed at around 475 cm^{-1} which corresponds to the shifting of the peak (at 375 cm^{-1}) of the Fe–O bond of magnetic support to a higher frequency. The silica network is adsorbed on the Fe_3O_4 surface by Fe–O–Si bonds. This adsorption band cannot be seen in the curve B to F because it seems at around 584 cm^{-1} and consequently overlaps with the Fe–O vibration of Fe_3O_4 MNPs. The strong absorption bands related to SiO_2 polymer onto the surface of Fe_3O_4 MNPs stretching vibrations are observed in the spectrum of SiO_2@Fe_3O_4 at 1112 and 985cm^{-1} assigned to the Si-O–H and Si–O–Si groups. The absorption bands at 919 and 808 cm^{-1} showed the presence of Si–OH stretching and OH vibrations on the surface of Fe_3O_4 MNPs (Fig. 1, curves B-F). Based on these observations, it was concluded that the formations of a continuous and very fine layer of silane on the surface of the Fe_3O_4 MNPs core (Fig. 1, curve. B). Several weak peak in the area of 1450–1560 $cm^{-1}$and 2860–2935 cm^{-1} are attributable to a propyl (C-H) stretching mode of carbon–carbon bond in 3-APTMS, and two peaks at 3460 and 1630cm^{-1} are ascribed to N–H stretching vibration NH_2 bending mode of free NH_2 group, that indicating amino-propyl groups are present at the ends of the Fe_3O_4 MNPs [15, 17, 32, 33]. The C=N imine vibration signal was observed at 1630 cm^{-1}, which shows the condensation reaction between CC with Si-APTMS@Fe_3O_4. The peaks at 1437-1434 cm^{-1} and 1251 cm^{-1} are attributed to the C=N stretching vibration and side chain in plane C–N–C and N–C–N bending of triazine ring, respectively [15, 31, 34]. When metformin reacts with CC on surface of modified magnetic support, Mn(II)-Met@MMNPs is formed. The peaks appeared at 1671 and 1650 cm^{-1} in curve F for the metal–ligand coordination presumably leads to a shift of these two peaks to lower frequencies. The weak absorption peaks at 413 cm^{-1} were appeared after complex formation of

Mn with immobilized metformin over modified Fe_3O_4 MNPs, which are related to the Mn-N band [15, 31, 35].

Selected images of SEM of Mn(II)-Met@MMNPs and parent support are shown in Fig. 2. It is obvious that morphology and size of particles of bulk magnetic support and Mn(II)-Met@MMNPs do not change as a result of their excellent chemical stability during the whole modification. The TEM images and DLS analysis shows that the average particle size in reverse micro emulsion solution of the manganese nanocatalyst were around 22 nm (Fig. 3). But the analysis of the Mn-nanocatalyst, which discloses the core/shell structure of the SiO_2@ Fe_3O_4, does not clearly show the Mn on its surface. Furthermore, comparison between TEM images of Fe_3O_4, Fe_3O_4@SiO_2 and Mn(II)-Met@MMNPs show an obvious SiO_2 as shell (around 4-8 nm-in-thickness) on Fe_3O_4.

EDX analysis of the Mn(II)-Met@MMNPs shows the presence of the Si and Fe elements corresponding to the magnetic support and also, manganese which confirm the composition of complex at modified support. The other signals as found in the EDX spectrum of the nanocatalyst were C, O, and N that show the chemical composition of synthesized organometallic support (see Fig. 4). Therefore, the mechanical and chemical stability and small nanoparticle size make Mn(II)-Met@MMNPs as a suitable nanocatalyst.

The crystalline phase and purity of the synthesized compound was indicated by the XRD (X-ray diffractometer) patterns (Fig. 5). The XRD pattern of magnetite Fe_3O_4 represented peaks at 2θ =18.2, 30, 35, 43, 54, 57 and 62.5. Those diffraction peaks correspond to the single spinal structure of Fe_3O_4 MNPs which attributed to (2 2 0), (3 1 1), (4 0 0), (4 2 2), (5 1 1) and (4 4 0) faces of crystal. The XRD pattern of SiO_2@Fe_3O_4 MNPs exhibited little broadened pattern due to its non-crystalline nature at 2θ = 15-30 and but show characteristic peaks at 30.2, 35.6, 43.3, 53.6, 57.3 and 62.8 which corresponded to the Fe_3O_4 MNPs structure (Fig. 5). Finally, the XRD patterns represent similar diffraction peaks which indicate that surface modification does not significantly effect on crystal structure of the magnetite nanoparticles. The XRD results confirmed that modified magnetic support structure by SiO_2 (as a coating amorphous agent) was maintained during subsequent synthesis steps [31]. In addition, the average grain size (D) of Mn(II)-Met@MMNPs was measured using the full width at half maximum (FWHM) from the Scherrer's equation ($D=K\lambda/(\beta \cos \theta)$), where k is the shape factor, λ is the wavelength of incident X-ray, b is the FWHM measured in radians and h is the Bragg angle of diffraction peak. The

average diameter of Mn(II)-Met@MMNPs was determined as about 22 nm from Scherrer's equation.

The electronic nature of functionalized Fe_3O_4 nanoproperties and its' immobilized Mn-metformin complex were elucidated by X-ray photoelectron spectroscopy (XPS). The C 1s and N 1s core level in NHPI and CC linker ligands generated peaks centered at 292 and 399 eV binding energy (Fig. 6). The peaks related to O 1s at Fe_3O_4 NPs, located in 536-542 eV binding energies (Fig. 6, a). The mixed oxidation state of Fe^{2+} and Fe^{3+} in Fe_3O_4 MNPs appeared at 720-710 eV related to Fe 2p core level (Fig. 6, b). The Fe $2p_{3/2}$ and $2p_{1/2}$ core level in Fe^{2+} at tetrahedral sites and their satellites locate at lowest binding energy in comparison with Fe^{3+} octahedral and tetrahedral species [36-39]. The Mn ($2p_{3/2}$) and Mn ($2p_{1/2}$) peaks related to Mn-N environment in Mn-metformin complex are located at 639 and 649 eV [40, 41].

Thermal stability of the synthesize manganese nanocatalyst was studied with derivative thermo gravimetric analysis (TG-DTG) in argon atmospheres. The TGA curves of the magnetic nanocatalysts show the mass loss of the organic materials as they decompose upon heating in the range of 25-1200 °C with a ramping rate of 10 °C/min (Fig. 7). As compared with TGA analyses of Fe_3O_4 and SiO_2@ Fe_3O_4 MNPs indicated negligible weight loss in the range of 25-1200 °C. TG-DTG analyses of Mn-immobilized complex shows three main weight loss steps from the samples as shown in Fig. 6. The Mn-nanocatalyst presents three distinct steps at 25–114, 255–385 and 351-1100 ˚C (Fig. 7). The first weight loss step observed at the temperature <114˚C (0.9% wt) on SiO_2@ Fe_3O_4 MNPs, which was related to the loss of physically adsorbed water from the surface of the catalyst. Stages II in weighting lost (155–351 °C) are due to desorption of water molecules from the SiO_2@ Fe_3O_4 MNPs core-shell NPs and also decomposition of the immobilized 3-APTMS groups. The additional weight losses in stage III could be observed due to the certain phenomena including desorption of closed water molecules in support, calcination of coke, loss of the new generated Si-OH groups and the decomposition of the immobilized manganese complex groups. The results reveal that the thermal stability SiO_2@ Fe_3O_4 core-shell is better than parent Fe_3O_4 MNPs. In addition, thermal stability of SiO_2@ Fe_3O_4 core-shell NPs in manganese nanocatalyst improved rather than unmodified SiO_2@ Fe_3O_4 core-shell NPs. These observations confirm the well grafting of organic groups on the magnetic support and indicate that the Mn(II)-Met@MMNPs has a good thermal stability which is probably due to strong interaction between the ligand and Fe_3O_4 MMNPs [15, 31].

The magnetic characterization of parent support and manganese nanocatalyst were carried out by vibrating-sample magnetometer at room temperature. As shown in figure 8, in the VSM magnetization curves of Fe_3O_4 and Mn(II)-Met@)MMNPs nanoparticles, there is no hysteresis and remanence and also, coercivity are negligible. The saturation magnetization value (Ms) of Mn(II)-Met@)MMNPs (41.2 emu/g) is lower than Fe_3O_4 (63.4 emu/g) due to the existence of non-magnetic SiO_2 coating. The Mn(II)-Met@)MMNPs nanoparticles exhibits superparamagnetic behaviour at room temperature although its Ms value is significantly less than pristine MMNPs. These data confirmed that both of the nanoparticles exhibit superparamagnetic behaviour.

3. 2. Catalytic performance study of immobilized Mn(II)-Met@)MMNPs

The selective and green oxidation of benzylic and allylic C-H bonds of abundant and simple material such as EB and CYHE represents a powerful processor for the synthesis of value-added products such as AcPO and CYHE=O. These products have widespread application in food industries (flavoring agent in foods), cosmetics industries (fragrance in soaps and perfumes), chemical industries (as a solvent for plastics and resins), and synthesis of a variety of chemical products such as pharmaceuticals insecticides, herbicides and fragrances. Therefore, catalytic performance of immobilized Mn(II)-Met@MMNPs was examined for the oxidation EB, CYHE and oximes by molecular oxygen as a green and eco-friendly oxidant.

3. 2. 1. Heterogeneous aerobic oxidation of EB catalyzed by immobilized Mn(II)-Met@)MMNPs

In continuation of our interest in exploring catalytic methodology [34-36], the selective aerobic oxy-functionalization of benzylic position in EB using novel heterogeneous magnetic nanocatalyst was investigated. The effects of various operating parameters, such as the amount of the nanocatalyst to NHPI, reaction temperature and time, solvent and radical inhibitor on the performance of the heterogeneous magnetic nanocatalysts were studied in aerobic oxidation of EB. In order to study the effects of solvents, a series of organic solvents, including aprotic aliphatics (cyclohexan, dichloromethane, trichloromethane, 1,2-dichloroethane, cyclohexane, acetonitrile), aprotic aromatics (toluene, benzene), protic aliphatics (methanol, ethanol, acetic acid), protic aromatic (benzylalcohol) and water was investigated to achieve a comprehensive understanding to the solvent role on the aerobic oxidation of EB. It seems that the viscosity and specific physical/chemical property (such as basicity and polarity) have main effect on

conversion and selectivity of desire products. Pervious study showed that the viscosity of organic solvent plays main roles in the liquid-phase reactions through altering the mass transfer, resulting in the different activity [42]. In the case of protic-OH containing solvents and water, EB and solvent molecules are in competition for the active sites of manganese center in catalyst. On the other hand by increasing of viscosity, the conversion of products is decreased (Table 2, entry 1-5). This decrement is due to the negative effect of viscosity on mass transfer in liquid phase. Polarity of solvent has a significant influence on the reactivity based on following reasons: (1) Stabilizing the intermediate radical species; (2) Enhancement of the formation and solubility of polar oxides; (3) enhance of desorption of polar oxide products to avoid blocking the active sites on manganese as active center in catalyst (Table 2, entry 6-10). Based on these results, it was found HOAc to be the suitable solvent. In fact, due to HOAc polar nature, solubility of NHPI increases in EB at the mild temperature employed in this protocol. Therefore, HOAc is necessary for observing an excellent catalytic activity. The EtOH and H_2O as electrons donor solvents had more ability to occupy the vacant space around the existing metal in nanocatalyst, therefor prevent to coordination of O_2 molecules to active catalytic sites.

Based on previous reports, AcPO, BZ-COH and PEA are major products in EB oxidation reaction [10, 15, 35]. While in this catalytic system, PEA, BZ-COH and oxidation product of the aromatic ring were not observed and AcPO was obtained as a sole product (Scheme 2).

In order to assess the effect of nanocatalyst on the catalytic activity and selectivity, the aerobic oxidation reaction of EB was investigated using different amount of Mn(II)-Met@MMNPs catalyst (Table 3). The oxidation in the absence of nanocatalyst has low conversion (8.0%) and selectivity (31.0 %) to AcPO at ambient temperature under O_2 bubbling (entries 1, 2).

It was observed that catalytic activity and selectivity is strongly affected by increasing amount of Mn(II)-Met@MMNPs to NHPI (entries 3-7) due to the presence of excess active nanocatalyst sites. In all EB aerobic oxidation reaction conditions by increasing of temperature, conversion and selectivity to AcPO increased with reaction time (entries 8-10). The most promising result is that by enhancing catalyst amount and temperature, AcPO is found to be the major product. Also, The EB oxidation was done in the presence of magnetic Fe_3O_4 NPs as catalyst and results show that the conversion was really negligible after 24 h (entry 11). These results confirmed the oxidation reaction could only proceed in the presence of the Mn(II)-Met@MMNPs, and there was no contribution from Fe_3O_4 NPs species as a catalyst in the aerobic oxidation reaction.

Concerning the catalytic pathway of EB oxidation using Mn(II)-Met@MMNPs heterogeneous nanocatalyst, Scheme 3 presents a reasonable proposed mechanism based on the precedent literature for similar nanocatalyst in hydrocarbon oxidation by dioxygen [34]. In contrast to catalyst that possess of transition metals, NHPI does not precipitate the hydroperoxide decomposition reaction. Hence, the catalytic activity of NHPI results from PINO (phthalimide-N-oxyl radical) formation in the aerobic oxidation process (scheme 3, Eq. 5). As a matter of fact, transition metals, such as Pd(II)/Pd(0), Mn(II)/(III) and Co(II)/(III), are usually applied as processes due to their catalytic effect which cause to decrease in activation energy of the decomposition reaction of the hydroperoxide. As it shown in the proposed mechanism in Eq. 5, the O_2 molecules coordinate to nanocatalyst in the presence of NHPI. In this step, NHPI could be converted to PINO by the reaction of NHPI with the Mn(III)-$OO^{\cdot}$ complex (superoxometal(III) or peroxometal(IV) complexes) that would be the most significant step in the present aerobic oxidation [33-36]. These results showed that manganese center is not occupied with the solvent or any other substrate and could coordinated with the dioxygene. In supplementary experiment for showing the role of the Mn(II)-Met@)MMNPs, pyridine molecule was added into the mixture of reaction which resulted in decreasing the catalytic activity of Mn(II)-Met@)MMNPs swiftly, in fact, the nitrogen of pyridine molecule versus oxygen easily occupies the Mn active sites in catalyst. In the equation 6, PINO will be generated that could abstract a hydrogen atom from EB and the stable aryl radical is produced. However obtaining the aryl radicals by O_2 molecules provides peroxy radicals (EB-$OO^{\cdot}$) which are eventually changed to oxygenated products through ethylbenzyl hydroperoxides (EB-OOH). The ethylbenzyl hydroperoxides in the next further converts to AcPO and PEA by Mn(III)-OOH (see Eq. 9 and 10). In equation 10 two alkylproxy radicals combine to form a tetroxide intermediate, which further decomposes via a six-membered ring transition state rearrange to a molecule of O_2, PEA and AcPO. This equation is well-known as Russell termination. It is expected from this mechanism that the ratio of PEA and AcPO are 1:1. During the first 2 h of the reaction, AcPO and PEA formation takes place only through Russell termination but at higher conversions, other path plays an important role. The EB-OOH was catalytically decomposed by the Mn(II)-Met@MMNPs. So, the selectivity of EB-OOH decreases after the increase of reaction time. However, in the presence of HOAc, the rate of this reaction increased and the selectivity of EB-OOH decreased, that is, the proton of HOAc can prompt decomposition of EB-OOH, and commonly this step becomes more fast [44-46]. The

high selectivity to AcPO and the absence of BZ-COH and PAD (2-phenylacetaldehyde) can be rationalized from the following discussion. EB molecules possess methyl and methylene group, the methyl group carries more number of hydrogen than the methylene group, which was not oxidized. The reasons for this result are: (1) the methyl group might be rotating more quickly than the methylene group; therefore its hydrogen was not abstracted by radicals, (2) the existence of different energy for barrier to rotation; therefore the hydrogens of methylene group were more readily available for radicals than methyl group [47, 48]. Base on above reasons, radicals abstract the hydrogens from the methylene group of EB and aryl radical was formed. Furthermore, the local magnetic field of Mn in nanocatalyst could be thought to retain the paramagnetic aryl radical until it is oxygenated by oxidant. And then, the produced free radical rapidly reacts by dioxygen to form EB-OO radical. In addition the oxidation of PEA might be more rapid than EB, as the rotation of –CHOH group is slower than the $–CH_2–$ group. Consequently, the hydrogen atom which reacted with Mn(III)-OO was expelled by radical in order to form AcPO (Scheme. 3, Eq.8).

3. 2. 2. Aerobic oxidation of cyclohexene catalyzed by modified magnetic Mn-nanocatalyst

Allylic oxidation of CYHE is an important process in chemical industries because this substance used as row materials for synthesis of variety products in the chemical industry [47]. In order to evaluate catalytic activity of the prepared magnetic Mn-nanocatalyst, the oxidation reaction of CYHE was studied in benzonitrile (PhCN) as solvent under O_2 bubbling (scheme 3).

Initially, the effective parameters at catalytic reaction were optimized at above mentioned conditions for aerobic oxy-functionalization of allylic position with different amounts of the catalyst, NHPI and solvents. The products of catalytic reaction including CYHE=O (2-cyclohexene-1-one), CYHE-OH (2-cyclohexene-1-ol) and CYHEP (cyclohexene epoxide), were identified by GC-Mass and quantified by GC (scheme 4). It was observed that CYHE conversion and selectivity of products changed with reaction time (25, 60, 80, 100 and 120 °C) under 15 % NHPI and molecular oxygen (Fig. 9). Surprisingly, the aerobic oxidation of CYHE proceeded even at ambient temperature to give CYHE=O in higher selectivity (74.7 %) after prolongs time. As the reaction time was raised from 2 to 24 h, the CYHE conversion and the selectivity to CYHE=O increased, while the selectivity to CYHEP and CYHE-OH were decreased at 100 °C (Fig. 9 a-c). In the aerobic oxidation of CYHE, all the reaction circumstances showed excellent

selectivity for the CYHE=O with only trace amounts of by-products being detected by GC-Mass after 24 h at 100 °C (see Fig. 9).

In order to study the main role of solvent in this reaction, various solvent such as PhCN (benzonitrile), ACN (acetonitrile), BZ (benzene) and DCM (dichloromethane) are selected. The maximum percentage of CYHE conversion in various solvents decreased in the following order: 96.4% (PhCN) > 47.0% (ACN) > 34.5% (DCM) > 11.8% (EtOH) > 0.0% (H_2O). The CYHE=O selectivity decreased with a protic solvent (PhCN, 97.0% > BZ, 53.4% > DCM, 41.0% > EtOH, 34.0% > H_2O, 0.0%). Therefore, dipole moments of the solvents probably played a main role in aerobic oxidation of CYHE. These result showed that the reaction in PhCN had high selectivity and more catalytic activity. These data confirmed that the CYHE and solvents were competing for occupation of the active sites on nanocatalyst. Manganese and other metal nanocatalyst are extensively applied in aerobic oxidation of various organic compounds because of their redox property and ability to demonstrate several valencies (Mn: (II), (III), (IV) and (VII)) with easy electron transfer between these states. The manganese spices as an active site in nanocatalyst has usually important role in these oxidation processes, wherein their catalytic effect lowers the activation energy of alkylhydroperoxide and allylhydroperoxide decomposition reaction. The difference behaviors of the metal ions may be a result of their different redox potentials and, in association with this, their different behaviors in catalyzing alkylhydroperoxide and allylhydroperoxide decomposition [40, 48]. The aerobic oxidation of CYHE in the absence of Mn(II)-Met@MMNPs and also, in the presence of Fe_3O_4 NPs given low conversion and selectivity to CYHE=O at 25, 60, 80,100 and 120°C.

In addition, no reaction was occurred in the absence of NHPI because radical formation is not occurring under this condition [35]. Therefore, these could be concluded from the observations that under above-mentioned reaction circumstance, the allylic hydrogen is more reactive than the C=C bond. However, the abstraction of hydrogen from the allylic carbon leads to allylic radical by PINO, which needs a lower activation energy than the transformation of C=C to epoxide. However, presence of 7-oxabicyclo[4.1.0]heptan-2-one as a result of the CYHE=O epoxidation, is not usually except in reactions with excellent conversion [48]. However, the catalytic oxidation with O_2 is usually a complicated process due to co-occurrence of several reactions (see Scheme 5). Initially, the Mn(II)-Met@MMNPs as an active site convert to peroxo or oxo-catalyst through interaction with dioxygen (Eq.12 and 13). The obtained products confirmed that

manganese hydroperoxo is an active intermediate species (Mn(III)–OOH) opposed to a manganese peroxo species (Mn–OO·). In our proposed mechanism, NHPI and CYHEP cause to formation of cyclohexene hydroperoxide (CYHE-HP), which can be used as oxidants for another epoxidation reaction with generation of epoxides and allylic alcohols (see Eq.6). Regarding the mechanism of oxygen transfer, the CYHE-HP has several potential routes in the catalytic oxidation reaction. In 16 equation, the CYHE-HP loss H_2O molecule and forms CYHE=O. Regarding the scheme 5, a tentative explanation is oxygen in CYHE-HP more electrophilic and labile to attack by an olefinic double bond and converting of CYHE to CYHEP by CYHE-HP [50-54]. It is worth to note that after 1 h, there were equivalent amounts of CYHE-OH and CYHE=O being formed, which is in agreement with the proposed mechanism where two cyclohexenyl peroxy(CYHE-OO·) radicals combine followed by decomposition of the resulting tetraoxide intermediate (Russel intermediate) into 1:1 ratio of the CYHE-OH and CYHE=O [55]. It is possible that the Mn(II)-Met@MMNPs catalyse oxidation via a radical-chain sequence pathway. Moreover, the radical nature of the olefin oxidation mechanism by the immobilized Mn(II)-Met@MMNPs was indicated by the interruption of an ongoing reaction after adding butylated hydroxytoluene (*BHT*) as radical scavenger (Eq.16, path A and C). It was observed that addition of 5 mol% BHT stopped the oxidative reaction and also did not change the ratio of products [56, 57]. We can also conclude that the pathway of allylic oxidation occurs via radical formation and the BHT reacts with free radicals, therefore delays oxidative processes. Also, after the addition of the radical scavenger, products distribution remained the same. Finally, CYHEP and CYHE-OH converted to CYHE=O via interaction with Mn(III)-OOH (Scheme 5, Eq.17 and 18).

3. 2. 3. Aerobic regeneration carbonyl compound from oximes catalyzed by Mn(II)-Met@MMNP heterogeneous nanocatalyst

The aerobic oxidation of substrates such as oxime to their corresponding carbonyl compounds has significant importance in fundamental research and industrial manufacturing. The world-wide annual production of carbonyl compounds is over 10^7 tones and many of these compounds are produced aldehydes or ketones from the oxidation of oximes. To explore the catalytic activity, the aerobic oxidation reaction of various oximes by Mn(II)-Met@MMNP heterogeneous nanocatalyst in presence of molecular oxygen as an ecofriendly oxidant was exanimated. The conversion and selectivity of catalytic oximes oxidation are dependent on a variety of parameters

such as solvent, amount of benzaldehyde, temperature and applied catalyst amount. Before carrying the detailed study on the catalytic oxidation of various oximes, as a preliminary study the reaction conditions were optimized by choosing acetophenone oxime as a model substrate.

For examining the role and effect of the solvent in the reaction, different solvents which are suitable at radical reactions [58] have been used, including PhMe, EtOH, MeOH, ACN, BZ, Cy and H_2O. The observations confirmed that in various solvents selectivity was 100 % and the maximum conversion decreased in the following order: PhMe (99.0)> ACN (81.0)> BZ (72.3)> Cy (18.0)> EtOH (8.2%)> MeOH (7.0%)> and H_2O (0.00). The aerobic oxidation in presence of coordinating solvents such as H_2O and MeOH made no reaction. It seems that the donor electrons in these solvent had more ability to occupy the vacant position around Mn as active sites in nanocatalyst. So, these lone pairs prevent from coordination of oxygen molecule as an oxidant. In this investigation, PhMe provided the highest conversion and selectivity to AcPO because it was reluctant to undergo free radical addition [59, 60]. Therefore, PhMe is an effective solvent for aerobic oxidation of acetophenoneoxime at a radical pathway.

The reaction temperature for accelerating the oxidation process was evidently effective. Accordingly, the temperature effects (30, 40, 50, 60 and 70 ˚C) were also monitored on the oxidation of model substrate under O_2 bubbling after 24 h in the presence of Mn(II)-Met@MMNP. It was observed that by increasing the reaction temperature to 50 ˚C, the conversions (86%) and also selectivity to AcPO (>90%) increase. Therefore raising temperature was effective for the aerobic catalytic process since the E_a (activation energy) was not sufficient for the catalytic reaction. If the oxygen molecules and substrate collide with enough kinetic energy and this energy is higher than the E_a, then the oxidation reaction occurs and AcPO forms. It seems that at 60 ˚C activation energy was sufficient for the catalytic circulation. By increasing the temperature up to 60 ° C, conversion increases favorably, but by increasing temperature more than 60 °C, a favorable effect won't be shown in conversion and selectivity, and also the side-products will be start to growth. So, temperature of 60 °C was chose as optimum temperature in this catalytic system.

For achieving highly efficient oxidation of oximes to carbonyl compounds, the presence of BZ-COH as an oxygen acceptor has determining role. The deoximation reaction stopped completely in the absence of BZ-COH even for 24 h that indicate Mn(II)-Met@MMNP catalyst have excellent performance for oxygen activation in the presence of BZ-COH. The result confirmed

that BZ-COH acts as oxygen acceptor molecule in deoximation reaction at this catalytic system (see Fig. 10).

For evaluating the catalyst role, different amount of Mn(II)-Met@MMNP was investigated in aerobic oxidation of model substrate with dioxygen using BZ-COH in the absence of Mn(II)-Met@MMNP (Table 3). The conversion of the AcPO from 6% in the absence of the Mn(II)-Met@MMNP, to higher than 99% in the presence of the Mn(II)-Met@MMNP indicated that the catalyst has an efficient and important role in deoximation by dioxygen. Also Fe_3O_4 NPs species was applied as a catalyst in deoximation of acetophenoneoxime .The conversion of the AcPO was less than 10%. These results confirm that the Mn(II)-Met@MMNP was necessary to proceed the catalytic reaction.

The maximum selectivity of carbonyl compound was obtained with the amount of 140 mg of the Mn(II)-Met@MMNP.

The regeneration of aldehyde and ketone from various oximes was examined under the above optimized reaction conditions (Table 4). The catalytic results show that Mn(II)-Met@MMNP is highly active catalysts in the heterogeneous oxidation process various oxime including both electron withdrawing and donating groups. It seems that electron donating groups in *ortho* and *para* position by enhancing nucleophilic attack to functional oxime group, significantly decrease catalytic reaction time (entries 1-8). Inter molecule hydrogen bonding in –OH group at *ortho* position by reducing electron density on oxime functional group, make reaction time longer (entries 12, 13). More number of electron donating group on aromatic ring, made oximes less attractive center to nucleophilic attack. Therefore, compelled reaction time took a long time (entry 14). In cinnamaldeydeoxime, C=N bond oxidation was done without interfering with other sensitive compounds conjugated C=C bonds and cinnamaldeyde is formed (entry 16). Furthermore, steric structure almost has no great effect on conversion and selectivity of oximes (entry 17). The efficiency of catalytic oxidation reaction seems very dependent on the electronic property of oximes. It is interesting to find that the obtained main products were nitrile rather than carbonyl compounds for the oximes with electron-withdrawing groups (entries 18-20). Meanwhile, the conversion and selectivity of nitrile was very low even with long reaction time, illustrating that electron- withdrawing effect retarded the regeneration of carbonyl compound.

A plausible catalytic reaction pathway which explains carbonyl and cyanide compound formation, is proposed in Scheme 6. This proposed mechanism indicates that the oxidation of

oxime with different groups on benzene ring go in different paths in the aerobic oxidation reaction. At first Mn(II)-Met@MMNP in the presence of O_2 produces an oxo-catalyst as intermediate. In oxo-catalyst production process, BZ-COH will be oxidized to the BZ-COOH (benzoic acid). Then, this oxo-catalyst attacks to the imine group in oxime via a nucleophilic attack. Through this step, oxime will be oxidized to its corresponding carbonyl compound and nitrile base on electron-donating and electron-drawing on benzene ring, respectively. The presence of electron-drawing groups in oxime (Entries 18-20) will change the path of catalytic reaction. So, as the speed of protonation of hydroxyl group in oxime will be more than the speed of Mn(III)-$O^{\cdot}$ nucleophilic attack to C=N bond [61, 62], consequently, nitrile was produced by the elimination of H_2O (Scheme 6, step7,8) . In addition for verify the kind of pathway reaction, BHT (*2,6-di-tert-butyl-4-methylphenol*), as a radical scavenger was added to mixture of reaction. As shown in scheme 6, aerobic oxidation was totally inhibited in the presence of BHT as a radical trap (step 9). This pathway reaction indicated that this work introduces an efficient method for an aerobic conversion of oximes to the corresponding carbonyl and cyanid compounds with Mn(II)-Met@MMNP as heterogeneous catalyst in the presence of BZ-COH.

Besides coordination to metformin ligand, the Mn ions may also coordinate with the Si–OH surface of support core-shell NPs. Therefore, the materials of blank support core-shell NPs that adsorbed Mn, were also utilized for aerobic oxidation experiment for EB, CYHE and acetophenonoxim as substratet. It turned out that the conversion (selectivity) of EB, CYHE and acetophenonoxim as substratet were almost 6.5% (13%), 15.5% (11%) and14.0% (91%), respectively. These observations are similar to the result of blank experiments. Therefore, in the aerobic oxidation of substrate with oxygen, the manganese ions absorbed on the surface of support core-shell NPs did not contribute in the aerobic oxidation process. The above results indicated that the oxidation occurs due to the catalytic nature of the chemically grafted of Mn onto the Met ligands in Mn(II)-Met@MMNP as a catalyst.

3. 2. 4. Recyclability study of immobilized Mn(II)-met complex

The reusability of synthesized heterogeneous Mn(II)-Met@MMNP catalyst was investigated in the oxidation of EB, CYHE and acetophenone oxime. After any catalytic oxidation reaction, the catalyst was simply separated, washed with fresh ethanol, ether and acetone, dried at 100 °C and then used for next aerobic oxidation reaction at same condition (Fig. 11). The results show

immobilized Mn(II)-Met@MMNP can reused seven cycles at acetophenone oxime oxidation, six cycles at CYHE and EB oxidation. In order to proof that the oxidation process was really catalyzed by heterogeneous Mn(II)-Met@MMNPs catalyst, the hot filtration test was applied. After the first catalytic reaction, the catalyst was simply immediately separated from the reaction mixture and then, fresh EB was added to the filtrate after the removal of Mn(II)-Met@MMNP and found that no more products were produced under the same conditions.

Also, leaching test was done after any catalytic reaction by examining filtrate by ICP analysis. The amount of leached manganese from heterogeneous catalyst was determined less than 0.01%. These results confirmed that the aerobic oxidation reaction catalyzed by heterogeneous Mn(II)-Met@MMNP

4. Conclusion

The selective oxidation of EB, CYHE and oximes by eco-friendly oxidant towards oxygenated derivatives produce significant value-chain chemical which are relatively inexpensive and accessible substrate can be converted into value-added products. In this regard, metformin-functionalized SiO_2@Fe_3O_4 core-shell NPs was successfully prepared by facile methods of chemical modification that exhibited excellent catalytic activity, selectivity, stability and recyclability in aerobic oxidation of EB, CYHE and various oximes. Characterization analyses of Mn(II)-Met@MMNPs nanocatalyst proved that manganese successful anchored on modified magnetic support and core/shell structure remains unchanged after the surface functionalization and oxidation process. Manganese on SiO_2@Fe_3O_4 MMNPs efficiently promote the aerobic oxidation of EB, CYHE and oximes to AcPO, CYHE=O and carbonyl corresponding compound, respectively, in the presence of molecular oxygen as ecofriendly and effective oxidant. Also aerobic oxidation of benzylic and allylic site were done with the molecular oxygen as a sole oxidant without the use of any reductant. The results showed that our catalytic system facilitated the generation of the actives species phtalimide-N-oxyl radical which further catalyzed the aerobic oxidation of EB and CYHE. In addition, we have presented a new, efficient and green methodology for the selective regeneration of aldehydes, ketones and nitriles from various oximes. High catalytic performance of Mn(II)-Met@MMNP could be mainly attributed to ultrafine size, high dispersion and uniform distribution of manganese nanoparticles on SiO_2@ Fe_3O_4 MMNPs high accessibility of the reactants. Finally, the mentioned process has advantages in terms of nano-heterogeneous nature, cheapness and availability of magnetic support, green

and selective process, easy recovery upto several cycle without significant loss of activity, chemical stability of the nanocatalyst, short reaction time, mild condition reaction, high conversion and selectively.

Acknowledgement

A.F. acknowledges research council of Pharmaceutical Sciences Branch, Islamic Azad University, for the research founding of this project.

References

[1] H. Cui, X. Gu, S. Lu, X. Fu, X. Zhang, G.Y. Fu, Z. Qiu, Q. Sui, Degradation of ethylbenzene in aqueous solution by sodium percarbonate activated with EDDS–Fe(III) complex, Chem. Eng. J. 309 (2017) 80-88.

[2] L.N. Andrade, S.F. Araujo, A.T. Matos, A.B. Henriques, L.C. Oliveira, P.P. Souza, P. Chagas, M.M.D. Leão, C.C. Amorim, Performance of different oxidants in the presence of oxisol: Remediation of groundwater contaminated by gasoline/ethanol blend, Chem. Eng. J. 308 (2017) 428-437.

[3] T. Zhu, H. Song, X. Dai, H. So, Preparation of Ni_2P/Al-SBA-15 catalyst and its performance for benzofuran hydrodeoxygenation, Chin. J. Chem. Eng. In Press, Accepted Manuscript, http://doi.org/10.1016/j.cjche.2017.03.027.

[4] X. Fu, X. Gu, S. Lu, M. Xu, Z. Miao, X. Zhang, Y. Zhang, Y. Xue, Z. Qiu, Q. Sui, Enhanced degradation of benzene in aqueous solution by sodium percarbonate activated with chelated-Fe(II), Chem. Eng. J. 285 (2016) 180-188.

[5] S. Lee, Z. Yu, N. Zaborenko, A. Varma, Acetophenone hydrogenation on Rh/Al_2O_3 catalyst: Intrinsic reaction kinetics and effects of internal diffusion, Chem. Eng. J. 288 (2016) 711-723.

[6] D. Wang, J. Li, Z. Xu, Y. Zhu, G. Chen, Preparation of novel flower-like $BiVO_4/Bi_2Ti_2O_7/Fe_3O_4$ for simultaneous removal of tetracycline and Cu^{2+}: Adsorption and photocatalytic mechanisms, J. Colloid Interface Sci. 533 (2019) Pages 344-357.

[7] H. Li, W. Xu, N. Wang, X. Ma, D. Niu, B. Jiang, L. Liu, W. Huang, W. Yang, Z. Zhou, Synthesis of magnetic molecularly imprinted polymer particles for selective adsorption and separation of dibenzothiophene, Microchim. Acta, 179 (2012) 123-130.

[8] J. Mondal, T. Senb, A. Bhaumik, Fe_3O_4@mesoporous SBA-15: a robust and magnetically recoverable catalyst for one-pot synthesis of 3,4-dihydropyrimidin-2(1H)-ones via the Biginelli reaction, Dalton Trans. 41(2012) 6173-6181.

[9] H. Yan, X.T. Qin, Y.Yin, Y.F.Teng, Z.Jin,C.J.JiaPromoted Cu-Fe_3O_4 catalysts for low-temperature water gas shift reaction: Optimization of Cu content, Appl. Catal. B: Env.226, (2018) 182-193.

[10] M. Sarno.M.Iuliano,Highly active and stable Fe_3O_4/Au nanoparticles supporting lipase catalyst for biodiesel production from waste tomato, Appl.Surface Science, 2018In Press, Corrected Proof, https://doi.org/10.1016/j.apsusc.2018.04.060.

[11] Q. Xia, Z. Jiang, D. Li,, J.Wang, Z. Yao,Green synthesis of a dendritic Fe3O4 @Feo composite modified with polar C-groups for Fenton-like oxidation of phenol, J.Alloys and Compounds, 746 (2018) 453-461.

[12] Y. Liu, J. Qiu, Y. Jiang, Z. Liu, M. Meng, L. Ni ,C. Qin, J. Peng, Selective Ce(III) ion-imprinted polymer grafted on Fe_3O_4 nanoparticles supported by SBA-15 mesopores microreactor via surface-initiated RAFT polymerization, Micropor. Mesopor. Mat**.** 234 (2016) 176-185.

[13] S. Urus, Synthesis of $Fe_3O_4@SiO_2@OSi(CH_2)_3NHRN(CH_2PPh_2)_2PdCl_2$ type nanocomposite complexes: Highly efficient and magnetically-recoverable catalysts in vitamin K3 synthesis, Food. Chem. 213 (2016) 336-343.

[14] A. Abdolmaleki, S. Mallakpour, M. Mahmoudian, M. R. Sabzalian, A new polyamide adjusted triazinyl-β-cyclodextrin side group embedded magnetic nanoparticles for bacterial capture, Chemical Engineering Journal, 309 (2017) 321-329.

[15] D. Habibi, A.R. Faraji, M. Arshadi, H. Veisi, A. Gil, Manganese nanocatalyst and N hydroxyphthalimide as an efficient catalytic system for selective oxidation of ethylbenzene, cyclohexene and oximes under aerobic condition, J. Molecular Catalysis A: Chemical**,** 382 (2014) 41-54.

[16] Jiatao Yu, Xiaohua Cao, Ming Lu, A novel and efficient catalytic system including TEMPO/acetaldoxime/$InCl_3$ for aerobic oxidation of primary amines to oximes, Tetrahedron Letters**,** 55 (2014) 5751–5755.

[17] D. Habibi, A.R. Faraji, M. Arshadi, S. Heydari, A. Gil, Efficient catalytic systems based on cobalt for oxidation of ethylbenzene, cyclohexene and oximes in the presence of N-hydroxyphthalimide, Appl. Catal. A: General**,** 466 (2013) 282–292.

[18] M. Hashimoto, Y. Eda, O. Yasutomo, I. Toshiaki, S. Aoki, A novel decarboxylation of α-amino acids: a facile method of decarboxylation by the use of 2-cyclohexene-1-one as a catalyst, Chemistry Letters. 15 (1986) 893–896.

[19] M. Liu, Z. Xiao, J. Dai, W. Zhong, Q. Xu, L. Mao, D. Yin, Manganese-containing hollow TS-1: Description of the catalytic sites and surface properties for solvent-free oxidation of ethylbenzene,Chemical Engineering Journal, 313 (2017) 1382-1395.

[20] W. Lv, L. Yang, B. Fan, Y. Zhao, Y. Chen, N. Lu, R. Li, Silylated MgAl LDHs intercalated with MnO_2 nanowires: Highly efficient catalysts for the solvent-free aerobic oxidation of ethylbenzene, Chemical Engineering Journal, 263 (2015) 309-316.

[21] R. Xie, G. Fan, L. Yang, F. Li, Hierarchical flower-like Co–Cu mixed metal oxide microspheres as highly efficient catalysts for selective oxidation of ethylbenzene, Chemical Engineering Journal, 288 (2016) 169-178.

[22] R. Rao, Q.Ling, H. Dong, X. Dong, Na Li, A. Zhang, Effect of surface modification on multi-walled carbon nanotubes for catalytic oxidative dehydrogenation using CO_2 as oxidant, Chemical Engineering Journal, 301 (2016) 115-122.

[23] M. Varyani, P. K. Khatri, S. L. Jain, Amino acid derived ionic liquid supported iron Schiff base catalyzed greener approach for the aerobic oxidation of amines to nitriles, Tetrahedron Letters 57 (2016) 723-727.

[24] Y. Zhang, F. Lu, R. Huang, H. Zhang, J. Zhao, Aerobic oxidation of amines to imines catalyzed by a ruthenium complex under solvent-free conditions, Catal. Commun. 81 (2016) 10-13.

[25] A.G. M. Silva, C.M. Kisukuri, T.S. Rodrigues, E.G. Candido, I.C. Freitas, A.H.M. Silva, J.M. Assaf, D.C. Oliveira, L.H. Andrade, P.H.C. Camargo, MnO_2 nanowires decorated with Au ultrasmall nanoparticles for the green oxidation of silanes and hydrogen production under ultralow loadings, Appli. Catal. B: Environmental, 184 (2016) 35-43.

[26] S. Debnath, S. K. Saxena, V. Nagabhatla, Facile synthesis of crystalline nanoporous $Mg_3(PO_4)_2$ and its application to aerobic oxidation of alcohols, Catal. Commun. 84 (2016) 129-133.

[27] N. Benferrah, M. Hammadi, C. Philouze, F. Berthiol, F. Thomas, Copper(II) complex of a Schiff base of dehydroacetic acid: Characterization and aerobic oxidation of benzyl alcohol, Inorg. Chem. Commun. 72 (2016) 17-22.

[28] C. Mu, K. Huang, T. Cheng, H. Wang, H. Yu, F. Peng, Silver-ethanolamine-formate complex based transparent and stable ink: Electrical assessment with microwave plasma *vs* thermal sintering, Chemical Engineering Journal, 306 (2016) 806-815.

[29] T.K.H Ta, M.T. Trinh, N.V. Long, T.T.M. Nguyen, T.L.T. Nguyen, T.L. Thuoc, B.T.Phan, D. Mott, S. Maenosono, H.T. Van, V.H. Le, Synthesis and surface functionalization of Fe_3O_4-SiO_2 core-shell nanoparticles with 3-glycidoxypropyltrimethoxysilane and 1,1′-carbonyldiimidazole for bio-applications, Colloids and Surfaces A: Physicochem. Eng. Aspects. 504 (2016) 376-383.

[30] A. R. Faraji, S. Mosazadeh, F. Ashouri, Synthesis and characterization of cobalt-supported catalysts on modified magnetic nanoparticle: Green and highly efficient heterogeneous nanocatalyst for selective oxidation of ethylbenzene, cyclohexene and oximes with molecular oxygen, J. Colloid Interface Sci. 506 (2017) 10-26.

[31] S. Liu, J. Fu, M. Wang, Y. Yan, Q. Xin, L Cai, Q. Xu, Magnetically separable and recyclable Fe_3O_4–polydopamine hybrid hollow microsphere for highly efficient peroxidase mimetic catalysts, J. Colloid Interface Sci. 469 (2016) 69-77.

[32] L. Zhang, B. Liu, S. Dong, Bifunctional Nanostructure of Magnetic Core Luminescent Shell and Its Application as Solid-State Electrochemiluminescence Sensor Material, J. Phys. Chem. B 111 (2007) 10448-10452.

[33] M. K. Yoo, I. Y. Kim, E. M. Kim, H.-J. Jeong, C.-M. Lee, Y. Y. Jeong, T. Akaike, C. S. Cho, Superparamagnetic Iron Oxide Nanoparticles Coated with Galactose-Carrying Polymer for Hepatocyte Targeting, J. Biomed Biotechnol. 2007 (2007) 1-9.

[34] S. Kakarndee, S. Nanan, SDS capped and PVA capped ZnO nanostructures with high photocatalytic performance toward photodegradation of reactive red (RR141) azo dyeJ. Enviro.Chem Eng, 6 (2018) 74-94.

[35] S. Mahmood, B.H.Xu, T.L. Ren, Z.B. Zhang, X. M. Liu, S. J. Zhang, Cobalt/N-Hydroxyphthalimide(NHPI)-Catalyzed Aerobic Oxidation of Hydrocarbons with Ionic Liquid Additive, Mol.Catal, 447 (2018) 90-96.

[36] D. Wilson, M.A. Langell, XPS analysis of oleylamine/oleic acid capped Fe_3O_4 nanoparticles as a function of temperature, Applied Surface Science, 303 (2014) 6-13.

[37] Z. Ozaydin, S. Yasyerli, G. Dogu, Synthesis and Activity Comparison of Copper-Incorporated MCM-41-Type Sorbents Prepared by One-Pot and Impregnation Procedures for H_2S Removal, Ind. Eng. Chem. Res. 47 (2008) 1035–1042.

[38] H.Y.L. Sylvia, Y.Y. Wang, C.C. Wan, Synthesis of PVP stabilized Cu/Pd nanoparticles with citrate complexing agent and its application as an activator for electroless copper deposition, J. Colloid Interface Sci. 310 (2007) 190–195.

[39] V.D. Chaube, S. Shylesh, A.P. Singh, Synthesis, characterization and catalytic activity of Mn(III)- and Co(II)-salen complexes immobilized mesoporous alumina, J. Mol. Catal A: Chem. 241 (2005) 79–87.

[40] Eugene S. Iltona, Jeffrey E. Postb, Peter J. Heaneyc, Florence T. Lingc, Sebastien N. Kerisita, XPS determination of Mn oxidation states in Mn (hydr)oxides, Applied Surface Science 366 (2016) 475–485.

[41] Radu Gavreaa, Cristian Leosteanb, Marin Coldeaa, Olivier Isnardc,d, Viorel Popa, Diana Benea, Effects of Co for Mn substitution on the electronic properties of $Mn_{2-x}Co_xVAl$ as probed by XPS, Intermetallics 93 (2018) 155–161.

[42] Y. Cao, H. Yu , H. Wang, F. Peng, Solvent effect on the allylic oxidation of cyclohexene catalyzed by nitrogen doped carbon nanotubes, Catalysis Communications 88 (2017) 99–103.

[43] X.J. Tang, J.H. Fei, Z.Y. Hou, X.M. Zheng, H. Lou, Characterization of Cu−Mn/Zeolite-Y Catalyst for One-Step Synthesis of Dimethyl Ether from $CO-H_2$, Energy & Fuels, 22 (2008) 2877-2884.

[44] P.J. Figiel, J.M. Sobczak, Aerobic oxidation of alcohols and alkylaromatics with dioxygen catalysed by *N*-hydroxyphthalimide with vanadium co-catalysts, New. J. Chem. 31 (2007) 1668-1673.

[45] P.A.Gunchenko, J. Li, B. Liu, H.Chen, A. E.Pashenko, V.V.Bakhonsky, T.S.Zhuk, A.A.Fokin, Aerobic oxidations with N-hydroxyphthalimide in trifluoroacetic acid, Mol. Catal, 447 (2018) 72-79.

[46] Y. Ishii, S. Sakaguchi, Recent progress in aerobic oxidation of hydrocarbons by *N*-hydroxyimides, Catal. Today, 117 (2006) 105-113.

[47] K.F. Podraza, Regioespecific alkylation of cyclohexenes; a review, Org. Prep. Proced. Int. 23 (1991) 217-235.

[48] Z.-W. Yang, Q.-X. Kang, H.-C. Ma, C.-L. Li, Z.-Q. Lei, Oxidation of cyclohexene by dendritic PAMAMSA-Mn(II) complexes, J. Mol. Catal. A: Chem. 213(2004) 169-176.

[49] S. M. Saqer, D. I. Kondarides, X. E. Verykios, Catalytic oxidation of toluene over binary mixtures of copper, manganese and cerium oxides supported on γ-Al_2O_3, Appl. Catal. B: Environ. 103 (2011) 275-286.

[50] W. Partenheimer, The Unusual Characteristics of the Aerobic Oxidation of 3,4-Dimethoxytoluene with Metal/Bromide Catalysts, Adv. Synth. Catal. 346 (2004) 1495-1500**.**

[51] A. Staykov, T. Miwa, K. Yoshizawa, Aerobic oxidation of alkanes on icosahedron gold nanoparticle Au55, J. Catal, 364 (2018)141-153

[52] M. Grinstaff, M. Hill, J. Labinger, H. Gray, Mechanism of catalytic oxygenation of alkanes by halogenated iron porphyrin, Science, 264 (1994) 1311.

[53] X. Lin, S. Jie, Z. Liu, Sulfur and nitrogen-doped porous cobalt carbon catalyst for high efficient aerobic oxidation of hydrocarbons, Mole. Catal, 455 (2018) 143-149.

[54] Y. Wen, J. Zhang, Q. Xu, X. T. Wu, Q.L. Zhu, Pore surface engineering of metal–organic frameworks for heterogeneous catalysis Coord.Chem. Rev, 376 (2018) 248-276.

[55] D. Habibi, A.R. Faraji ,M. Arshadi, J.L.G. Fierro, Characterization and catalytic activity of a novel Fe nano-catalyst as efficient heterogeneous catalyst for selective oxidation of ethylbenzene, cyclohexene, and benzylalcohol**,** J. Mol. Catal. A: Chem. 372 (2013) 90-99.

[56] R. Luque, S.K. Badamali, J.H. Clark, M. Fleming, D.J. Macquarrie, Controlling selectivity in catalysis: Selective greener oxidation of cyclohexene under microwave conditions, Appl. Catal. A General, 341 (2008) 154-159.

[57] B. N.Echevarría, E. Goicoechea, M.D. Guillén, Polyunsaturated lipids and vitamin A oxidation during cod liver oil in vitro gastrointestinal digestion. Antioxidant effect of added BHT, Food. Chem, 232 (2017) 733-743.

[58] J.S. Uber, Y. Vogels, D. Helder, I. Mutikainen, U. Turpeinen, W.T. Fu, O. Roubeau, P. Gamez, J. Reedijk, Pyrazole-Based Ligands for the [Copper–TEMPO]-Mediated Oxidation of Benzyl Alcohol to Benzaldehyde and Structures of the Cu Coordination Compounds, Eur. J. Inorg. Chem. 2007 (2007) 4197-4206.

[59] J.M. James, 57J.O. Philip, A.U .Gregg, L. Bruno, P.C Dennis, Modern Solvents in Organic Synthesis; Springer: New York, 1999.

[60] X. T. Zhou, Q.L. Yuan , H. B. Ji, Highly efficient aerobic oxidation of oximes to carbonyl compounds catalyzed by metalloporphyrins in the presence of benzaldehyde, Tetrahedron lett. 51 (2010) 613-617.

[61] A. García-Ortiz, A. Grirrane, E.Reguera, H. García, Mixed (Fe^{2+} and Cu^{2+}) double metal hexacyanocobaltates as solid catalyst for the aerobic oxidation of oximes to carbonyl compoundsJ. Catal, 311 (2014) 386-392.

[62] F.P. Silvaa, R.V. Gonc¸ Goncalves, L.M. Rossia, Magnetically recoverable copper oxide catalysts for aerobic allylic oxidation of cyclohexene, J. Mol. Catal. A: Chem. 426 (2017) 534–541.

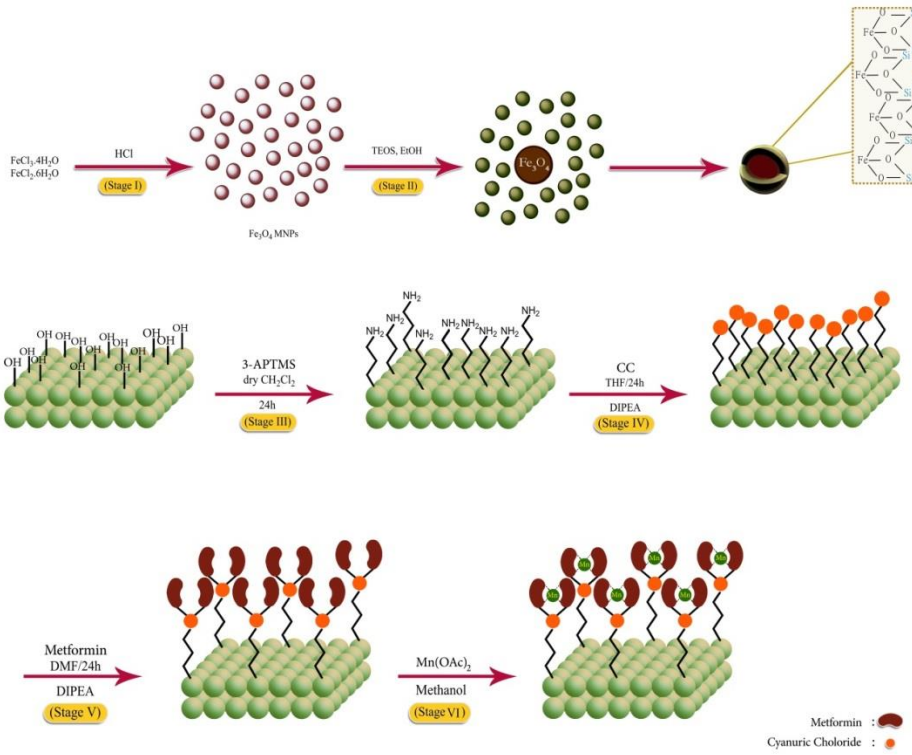

Schem 1. Schematic presentation of consequence synthesis process of supported Mn-metformin complex on modified magnetic SiO_2@Fe_3O_4 core/shell.

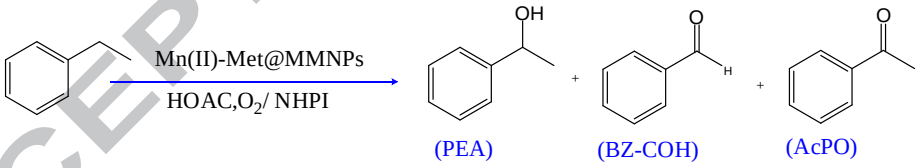

Scheme 2. Possible products of aerobic oxidation of EB catalyzed by immobilized Mn-nanocatalysts.

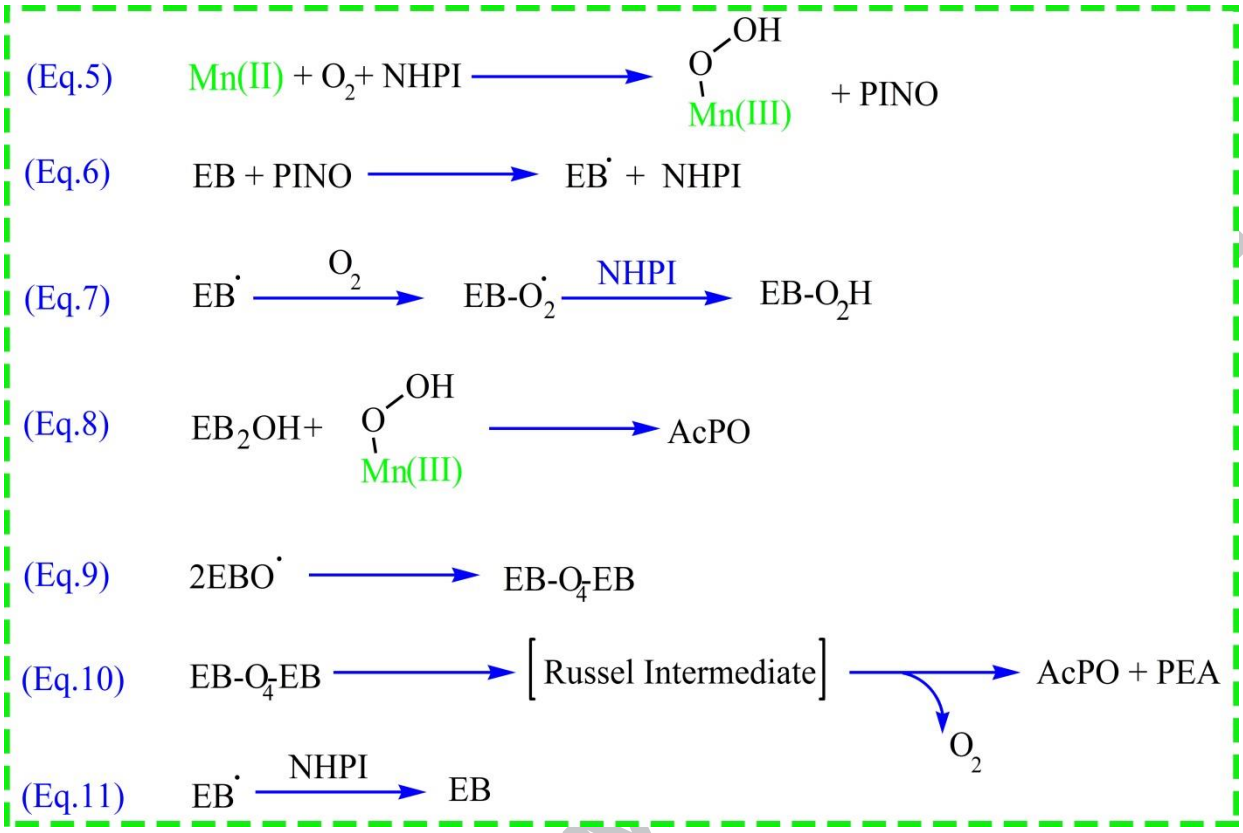

Scheme 3. Proposed pathway for EB oxidation to AcPO by Manganese/NHPI/ O_2 system.

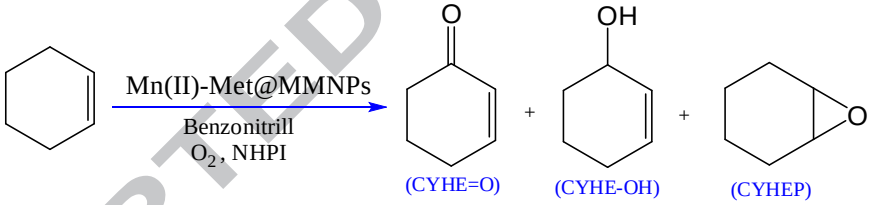

Scheme 4. Reaction products of catalytic oxidation of cyclohexene using Mn(II)-Met@MMNPs.

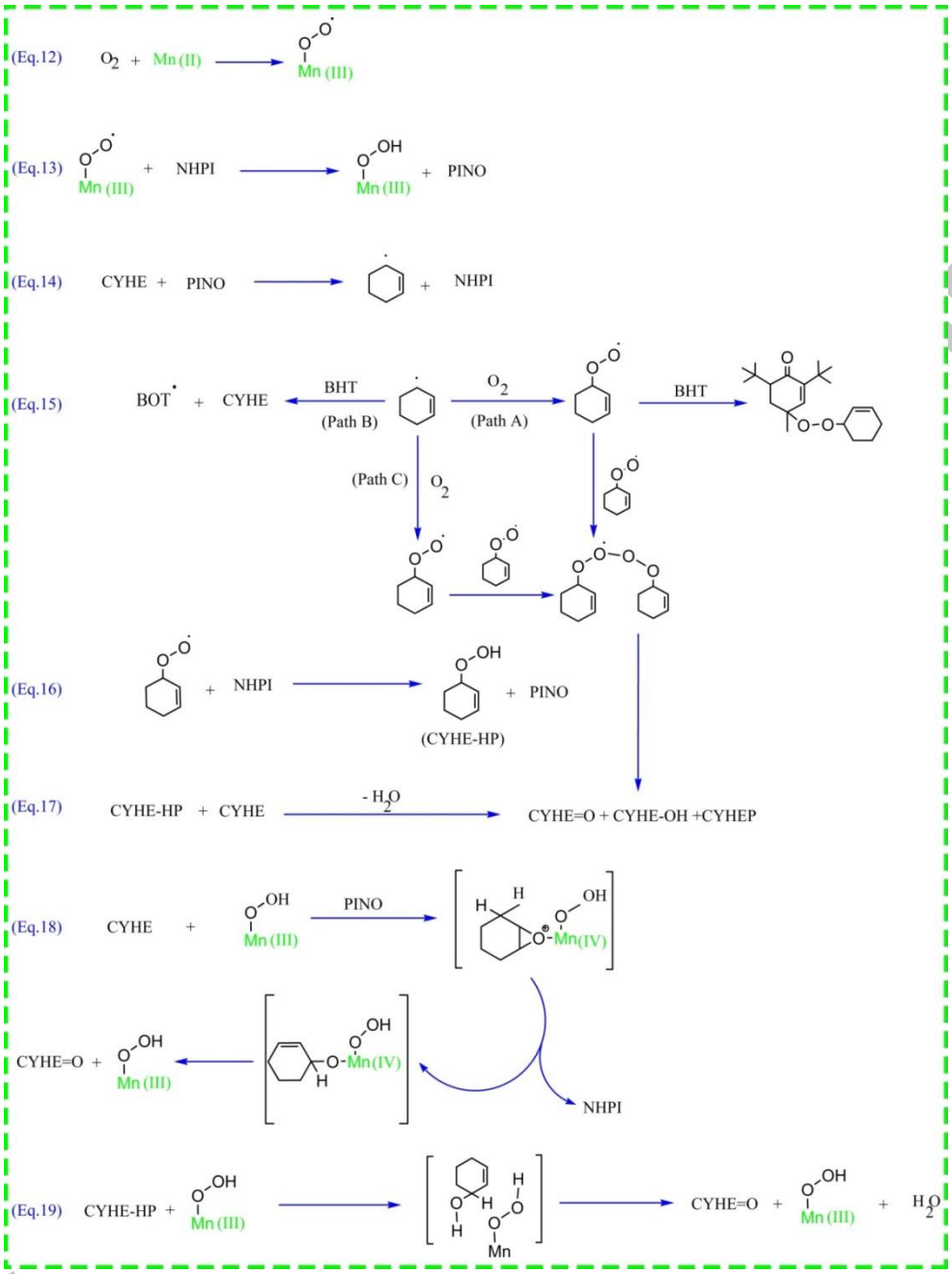

Scheme 5. Proposed pathway for the selective aerobic oxidation of CYHE to CYHE=O with Manganese/NHPI system.

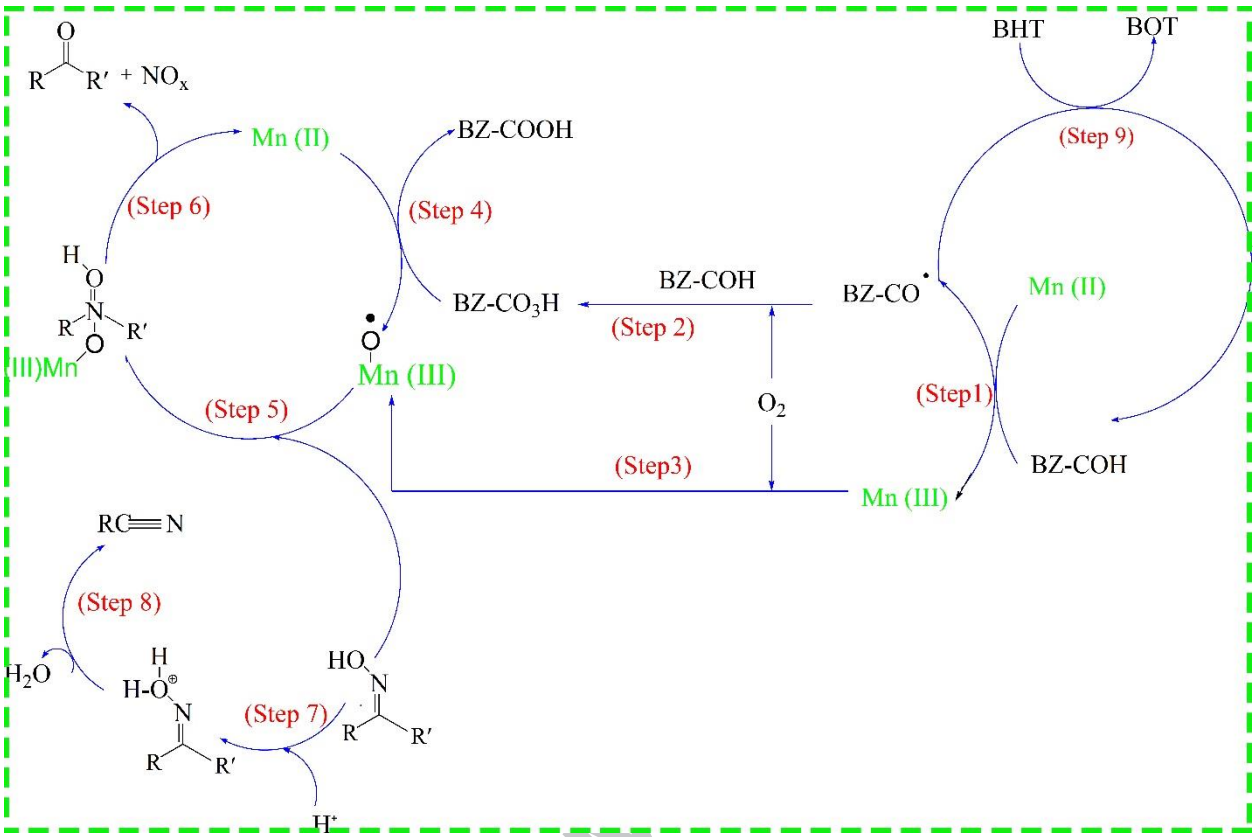

Scheme 6. Proposed pathway for the aerobic conversion of oximes to corresponding carbonyl or nitrile compound by Manganese/NHPI/BZ-COH system.

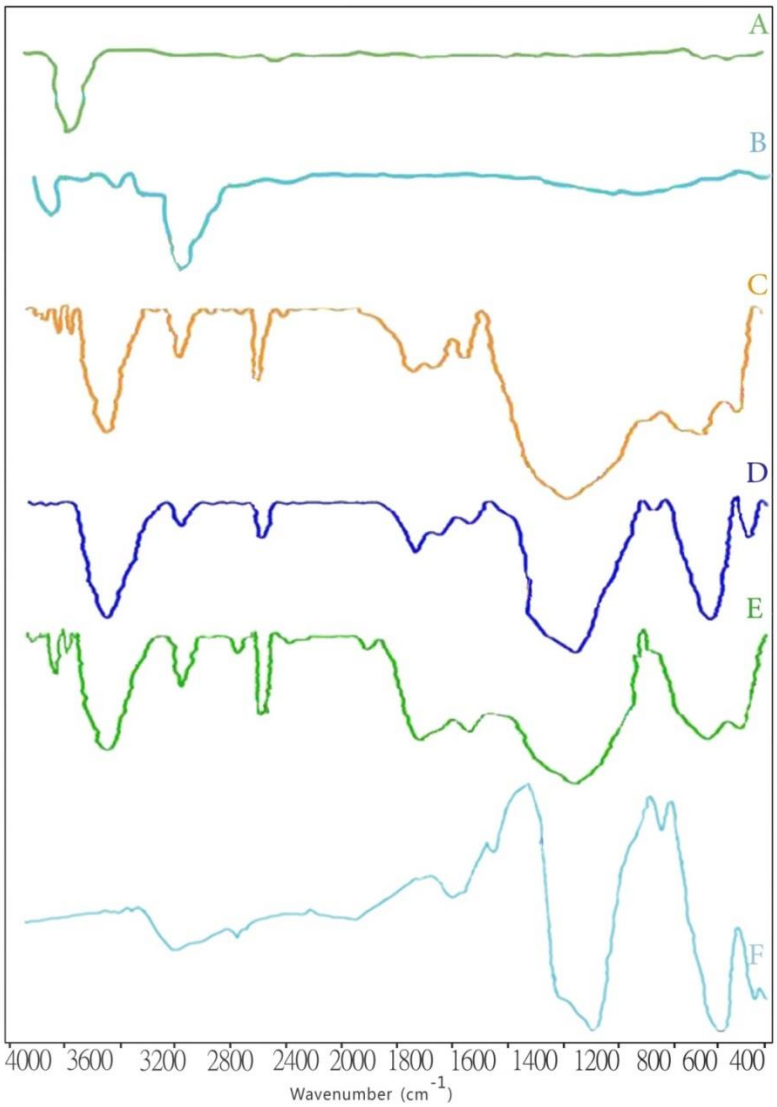

Fig. 1. FT-IR spectra of: (**A**): Fe_3O_4 MNPs, (**B**): $SiO_2@Fe_3O_4$, (**C**): $SiO_2@Fe_3O_4$ supported APTMS, (D): $SiO_2@Fe_3O_4$ supported APTMS/CC, (E): Met@MMNPs and (F): Mn(II)-Met@MMNPs.

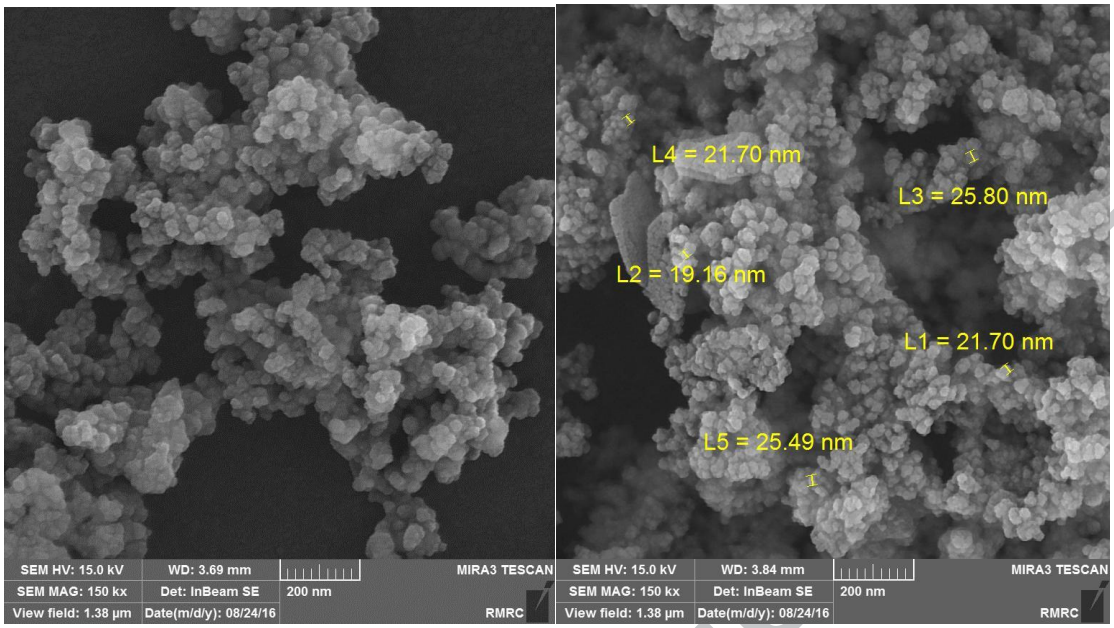

Fig. 2.SEM images corresponding to (A): Fe_3O_4 MNPs; (B): Mn(II)-Met@MMNPs.

Fig. 3.

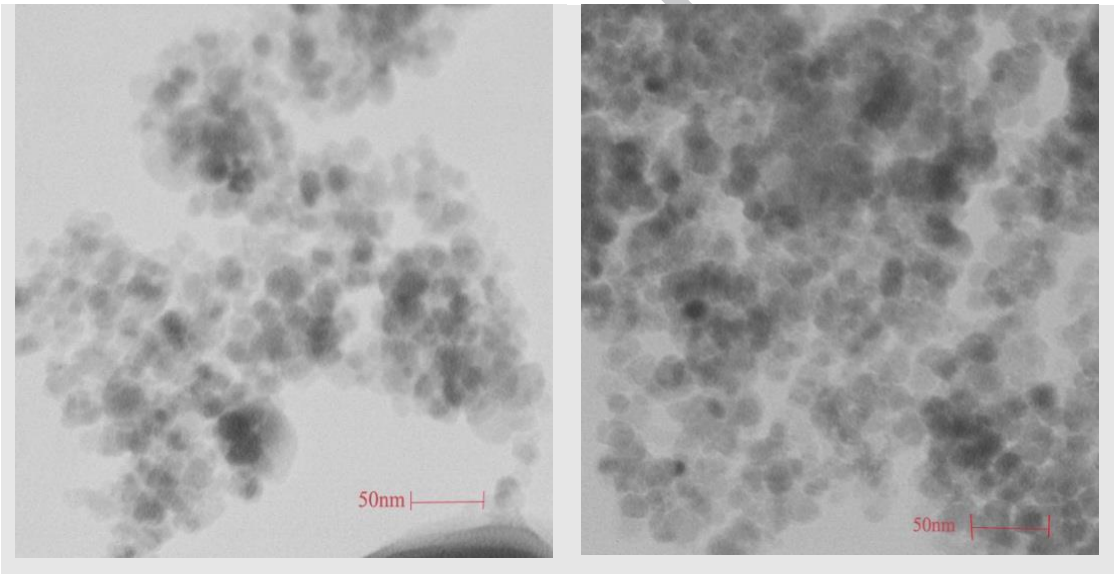

TEM images of synthesized Mn(II)-Met@MMNPs catalyst.

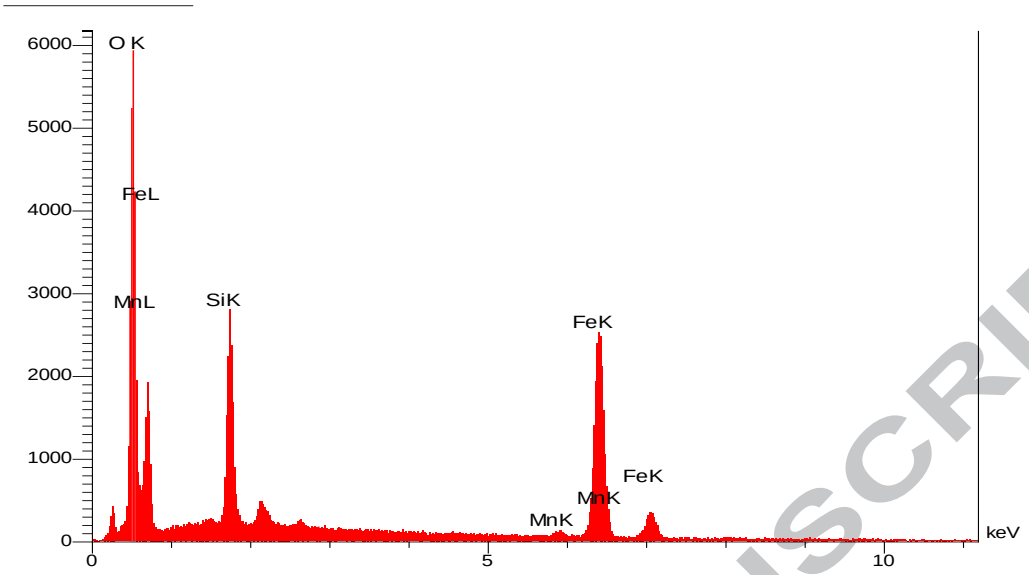

Fig. 4. EDX spectrum of synthesized Mn(II)-Met@MMNPs.

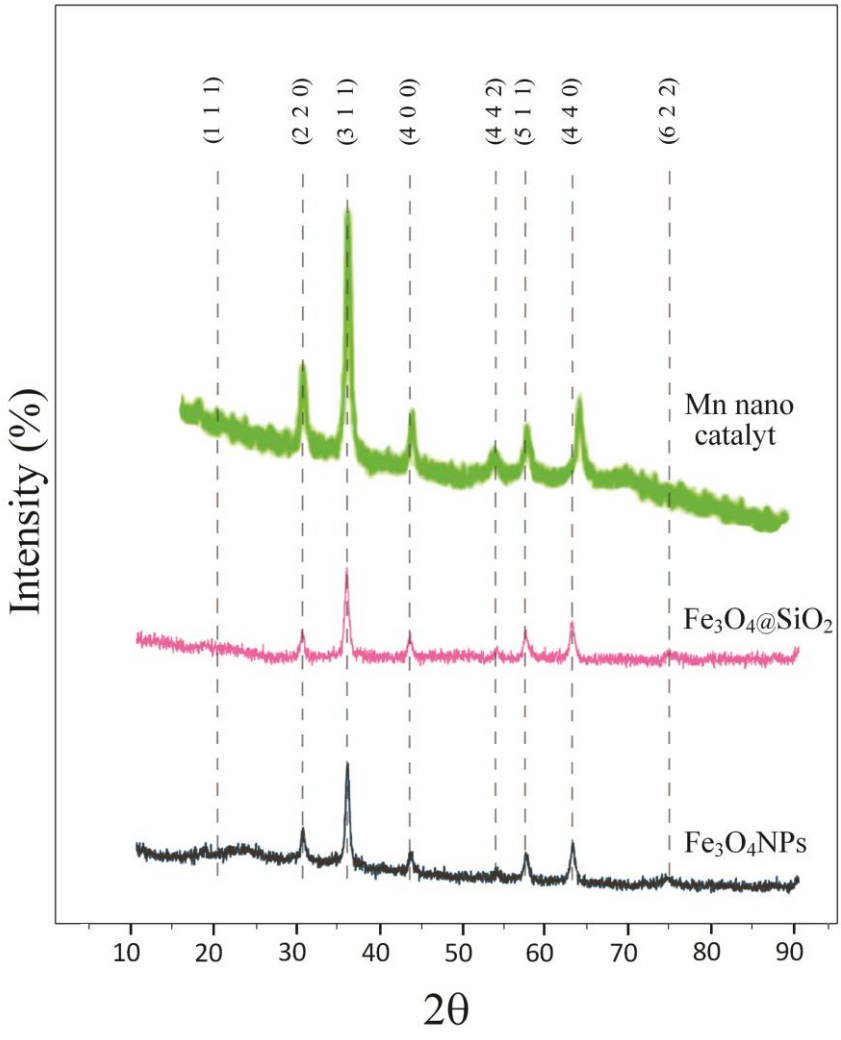

Fig. 5. XRD spectrum of Fe_3O_4 MNPs, SiO_2@Fe_3O_4 MNPs and Mn(II)-Met@MMNPs.

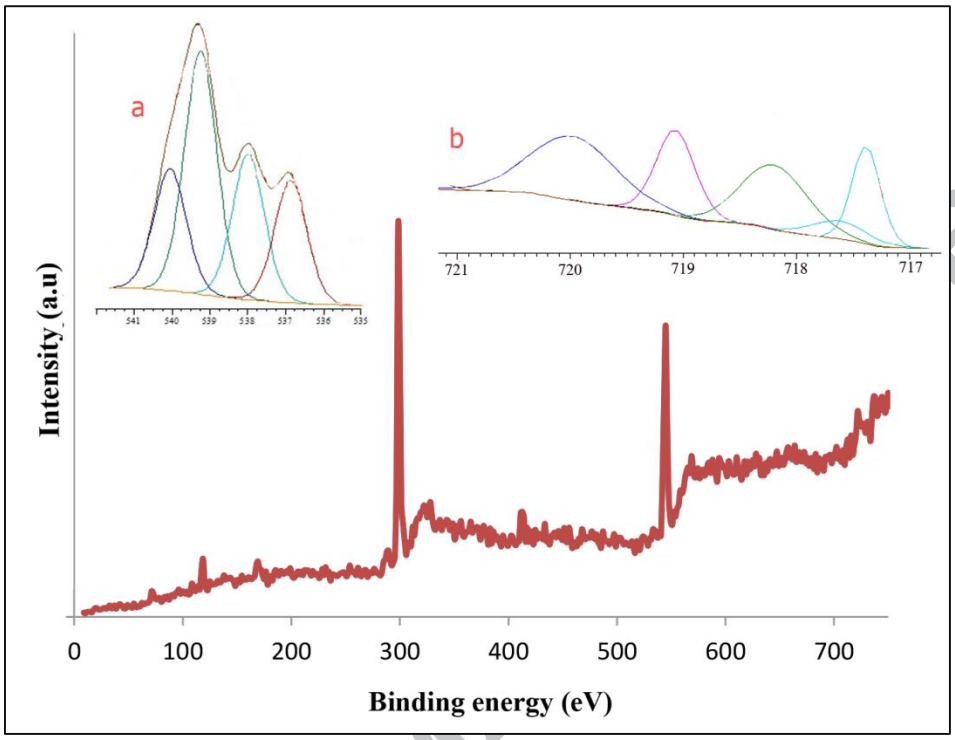

Fig. 6. The expand XPS image of Mn(II)-Met@MMNPs with core level related to oxygen (a) and iron (b) at modified Fe_3O_4 MNPs.

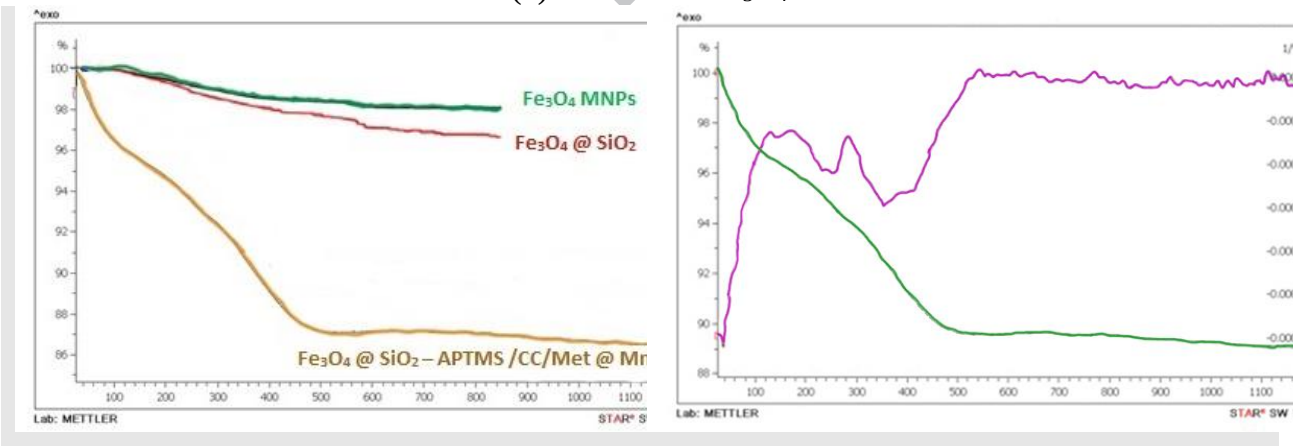

Fig.7. TGA and TG-DTG profile of (A): Fe_3O_4 MNPs, Fe_3O_4 MNPs@SiO_2 and Mn(II)-Met@MMNPs (II); (B): DTG of Mn(II)-Met@MMNPs.

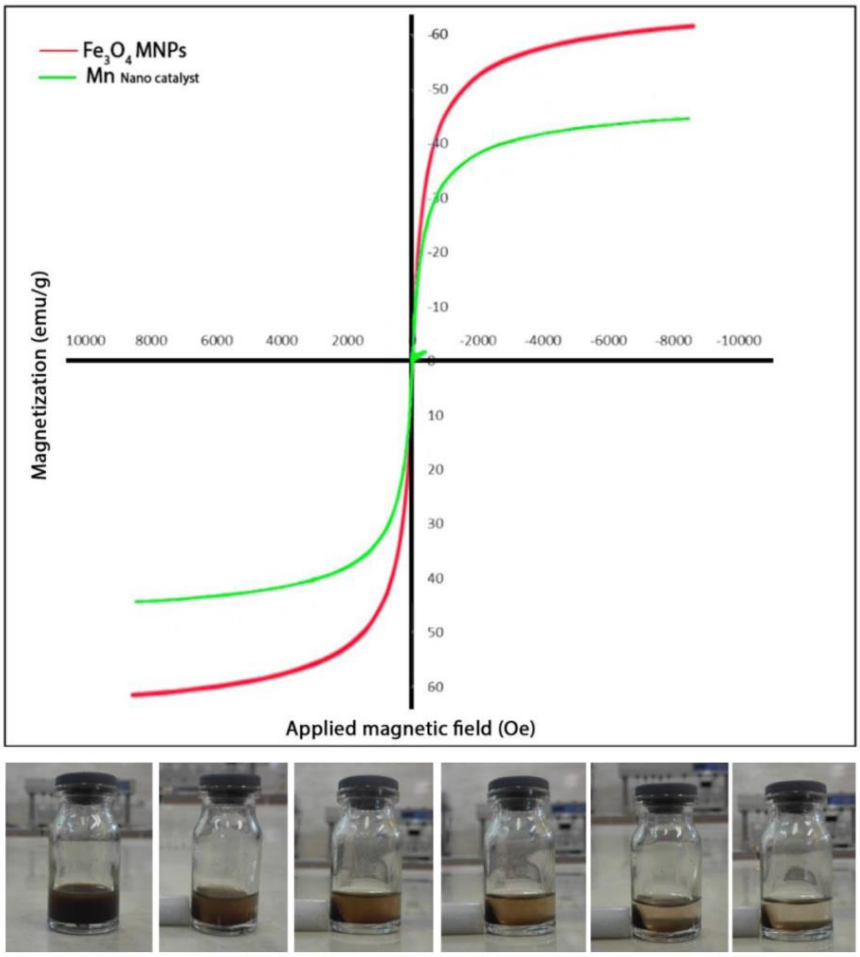

Fig. 8. The VSM spectra of Fe_3O_4 and Mn-nanocatalyst and separation of magnetic heterogeneous nanocatalyst from reaction mixture by the external magnet.

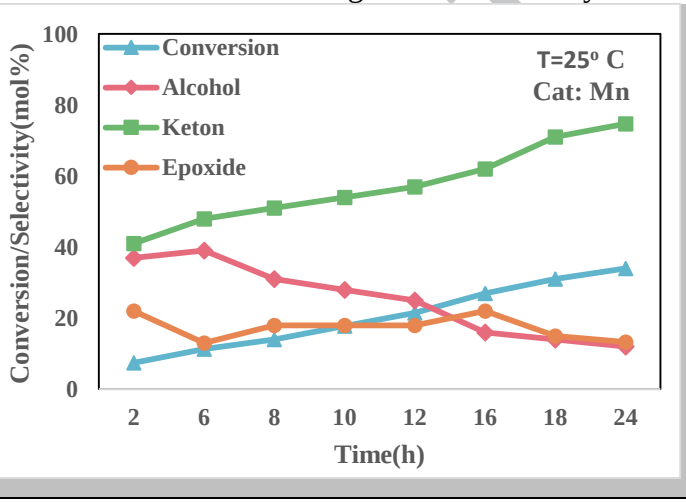

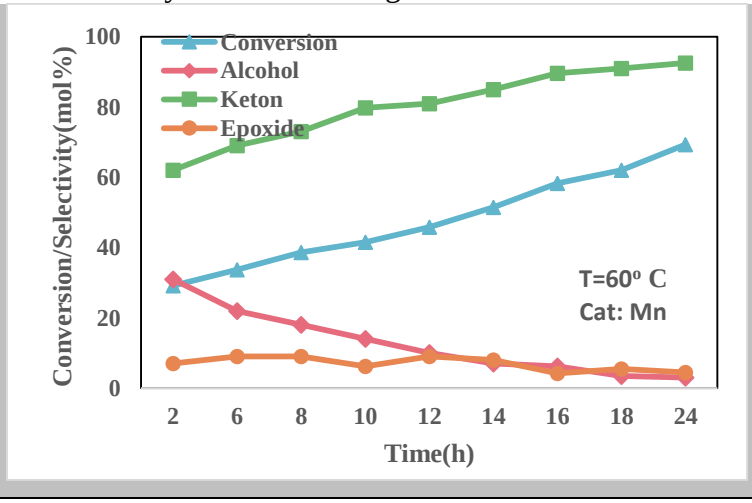

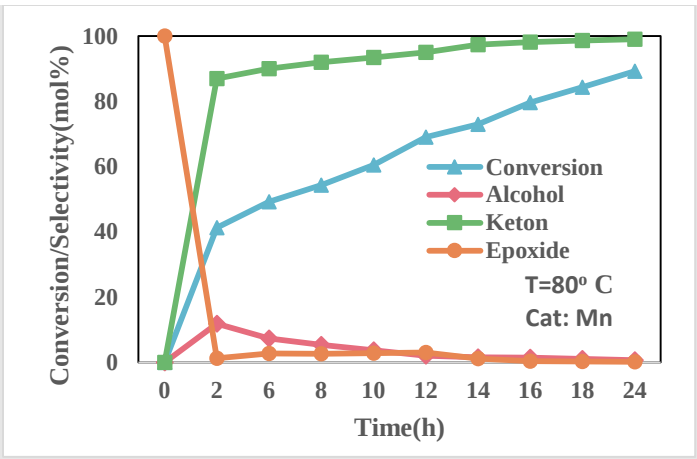

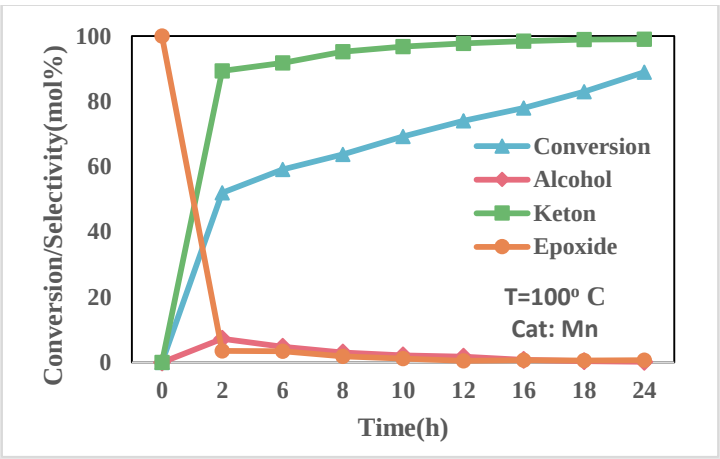

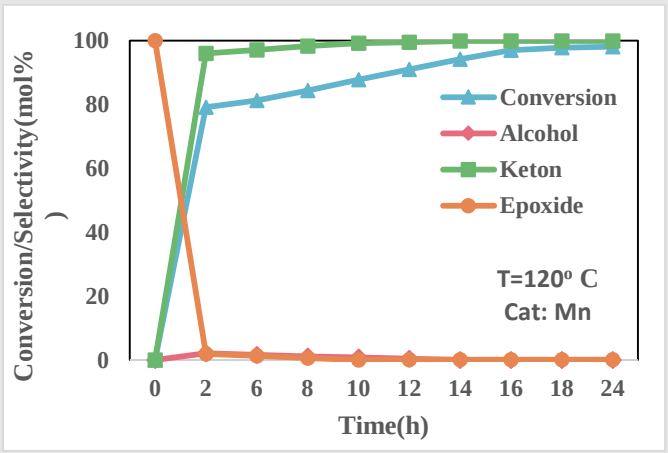

Fig. 9. The influence of reaction temperature on selectivity and conversion of cyclohexen oxidation and selectivity to 2-cyclohexene-1-one using Mn(II)-Met@MMNPs.
Reaction conditions: CYHE, 2 mL; Cat., 100 mg; solvent, benzonitrile; 15 mol% NHPI.

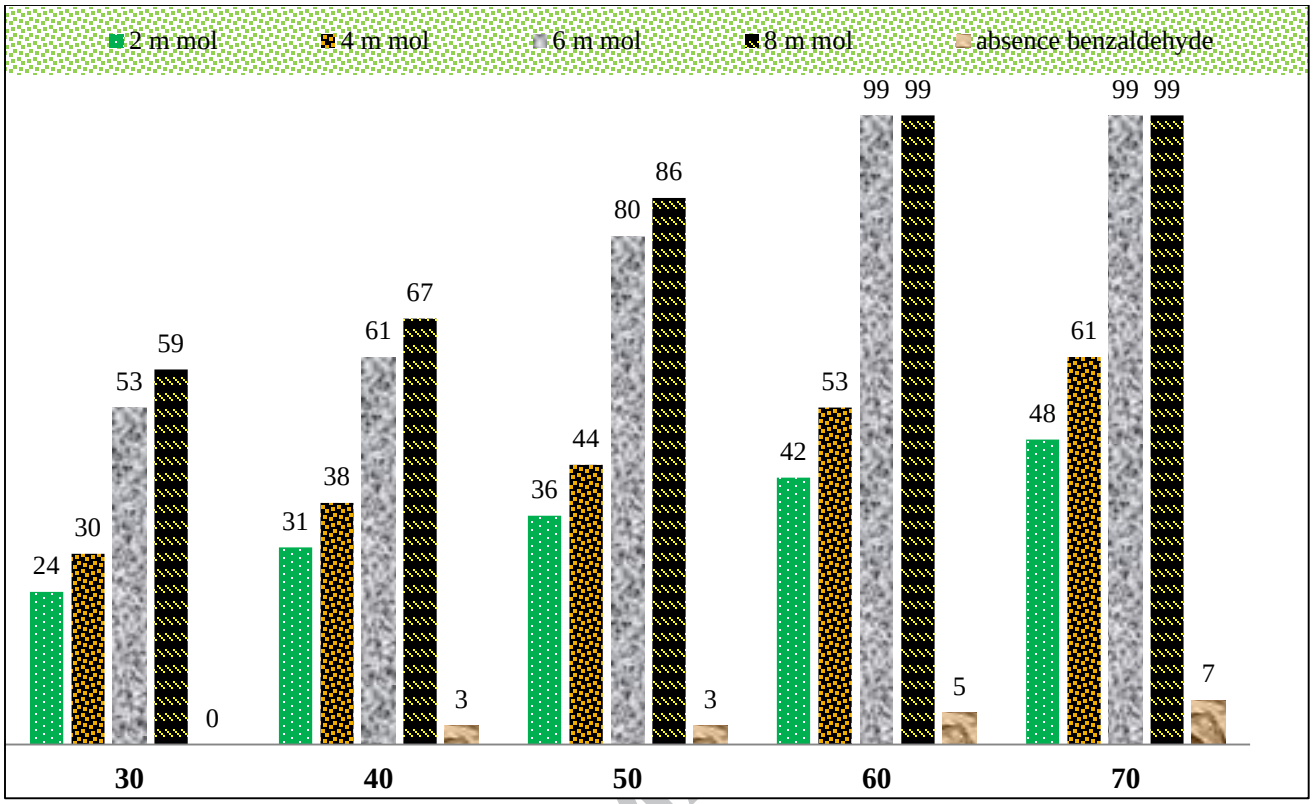

Fig. 10. The influence of amount of benzaldehyde on the acetophenone oxime oxidation to acetophenone by the Mn-nanocatalyst.

Reaction conditions: Acethophenonoxim, 2 mmol; Cat., 140 mg; Toluene, 5 ml; T = 60 °C; under O_2.

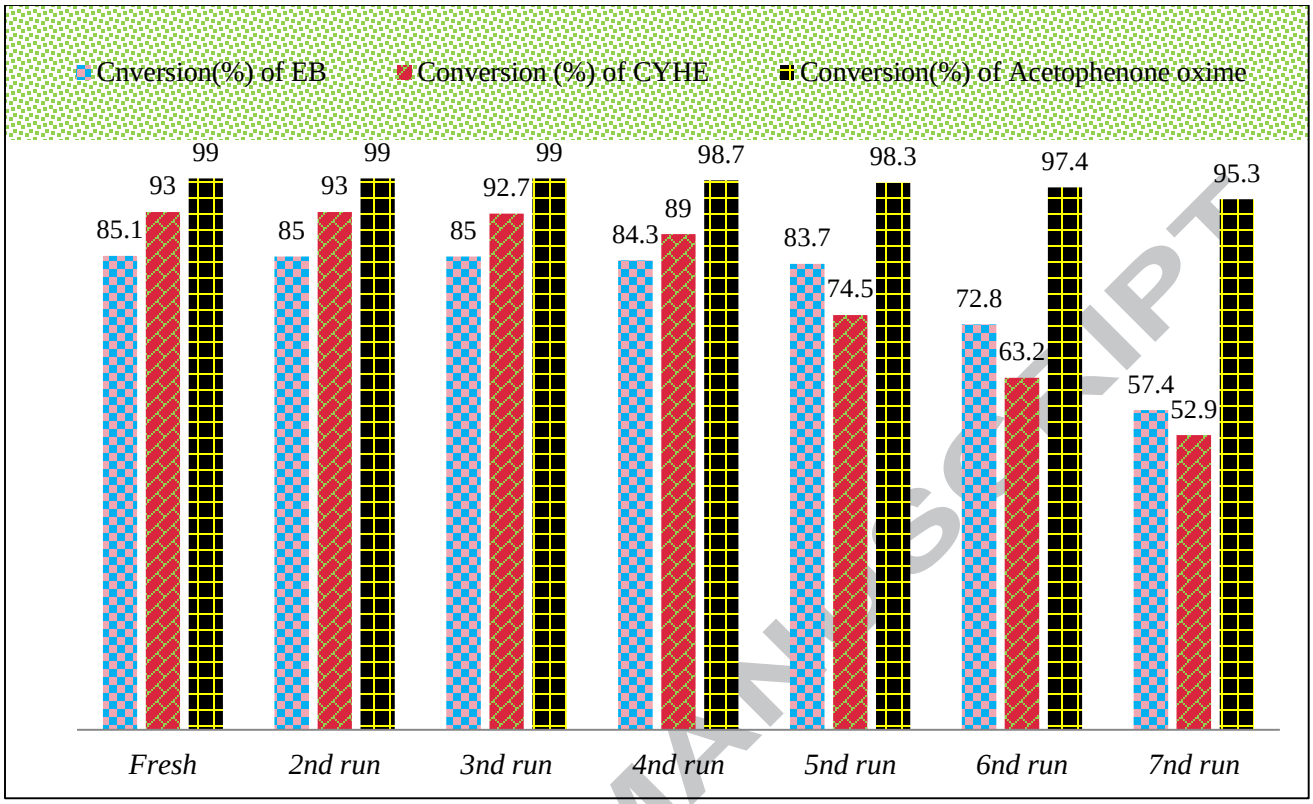

Fig. 11. Reusability of the Mn-nanocatalyst in the oxidation of ethylbenzene, cyclohexen and acetophenone oxime.
Reaction conditions:
EB, 2 mL; Cat., 100 mg; Acetonitrile, 5mL; 15 mol% NHPI, T = 100 °C; under O_2 bubbling.
CYHE, 2 mL; Cat., 100 mg; Benzonitrile, 6mL; 15 mol% NHPI, T = 120 °C; under O_2 bubbling.
Oxim, 2 mmol; Cat., 140 mg; Benzaldehyde, 5mmol; toluene, 6 ml; T = 60 °C; under O_2 bubbling.

Table 1. Structural parameters of MMNPs and immobilized Mn-metformine complex[a].

[a]From N_2 adsorption/desorption experiments.

Sample	S_{BET} (m^2/g)	V_{BJH} (cm^3/g)	*MPD* (nm)
SiO_2 @Fe_3O_4	71.1	0.17	8.45
SiO_2-ATPMS@Fe_3O_4	54.2	0.11	13.1
Met@MMNPs	39.8	0.09	21.6
Mn(II)-Met@MMNPs	24.6	0.05	25.4

Table. 2. The aerobic oxidation of EB catalyzed by Mn(II)-Met@MMNPs catalyst.

Entry	Solvent[a]	Conversion (%)	TON[b]	Selectivity (%)		
				AcPO	PEA	BZ-COH
1	Methanol	25.1	3038.7	34.7	45.2	19.2
2	Ethanol	13.4	1622.3	27.2	54.1	18.3
3	Water	0.0	-	0.0	0.0	0.0
4	Acetic acid	85.1	10302	98	1.8	Trace
5	Benzyl alcohol	10.6	1283.3	27.2	54.9	16.4
6	Di-chloromethane	38.3	4636.8	40.1	37.2	21.5
7	Tri-chloromethane	40.1	4854.7	45.2	39.1	15.2
8	1,2-Dicholoroethan	38.2	4624.7	39.3	24.1	35.7
9	Cyclohexane	47.1	5702.2	37.2	43.2	18.4
10	Acetonitrile	51.5	6234.7	48.2	31.5	19.4
11	Toluene	35.2	4261.5	15.4	32.7	49.1
12	Benzene	29.4	3559.3	52.6	31.2	11.9
13	Acetic acid[c]	trace	-	-	-	-
14	Acetic acid[d]	trace	-	-	-	-

[a]Reaction conditions: EB, 2 mmol; Cat., 100 mg, solvent, 5mL; 15 mol% NHPI, T = 100 °C; under O_2 bubbling.

[b]TON: Turn Over Number= moles of substrate converted per mole of metal.

[c]The reaction was done in the absence of Mn(II)-Met@MMNPs catalyst**.**

[d]The reaction was proceed by the use of Fe_3O_4 NPs as a catalyst**.**

Table 3. Effect of temperature and amount of catalyst on the conversion and selectivity of the aerobic oxidation of EB catalyzed by Mn(II)-Met@MMNPs nanocatalyst.

Entry	**Catalyst (mg)**	***t* (h)**	**T (ºC)**	**Conversion (%)**	**TON[b] (TOF)[c]**	**Selectivity (mol%)** AcPO	PEA Bz-COH
1	-	24	25	6	-	31	55 10
2	-	24	80	9	-	32	57 12
3	20	8	25	18	6053 (756.6)	42	40 16
4	30	8	25	22	8878 (1109)	59	25 14
5	50	8	25	25	5326 (665.7)	63	25 11
6	100	12	25	27	3292 (274.3)	61	23 13

7	150	12	25	34	2747 (228.9)	67	23 10
8	50	10	80	37	8958 (895.8)	78	14 7
9	100	8	80	82	9963 (1245)	98	2 -
10	100	8	100	85	10302 (1287)	98	2 -
11	100[d]	24	100	trace	-	-	- -

[a]Reaction conditions: Cat.,100 mg; EB, 2 mmol; NHPI, 15 %; HOAc, 5 ml ; under O_2 bubbling.
[b]TON: Turn Over Number= moles of substrate converted per mole of metal.
[c]TOF: Turn Over Frequencies (min^{-1}).
[d]The reaction was done by Fe_3O_4 NPs as a catalyst.

Table 4. Aerobic oxidations of oximes using Mn(II)-Met@MMNPs nanocatalyst.

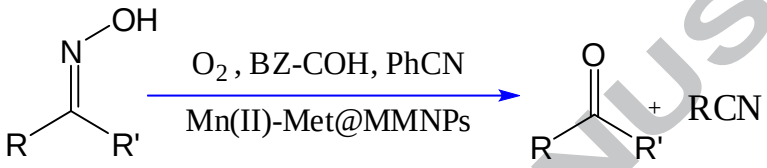

Entry	Substrate[a]	Product (selectivity %)	*t* (min)	Con. (%)	TON[b]	TOF[c]
1	Acetophenoneoxime	Acetophenone (100)	60	>99	8561	142.6
2	4-Bromobenzaldehyde oxime	4-Bromobenzaldehyde (100)	65	96	8301	127.7
3	3- Bromobenzaldehydeoxime	3- Bromobenzaldehyde (100)	65	99	8561	131.1
4	3- Methylbenzaldehydeoxime	3- Methylbenzaldehyde (100)	80	>99	8561	107.0
5	4- Methylbenzaldehydeoxime	4- Methylbenzaldehyde (100)	90	97	8388	93.20
6	4- Methylacethophenonoxime	4- Methylacethophenon (100)	100	96	8301	83.01
7	4-Choloro benzaldehyde oxime	4-Choloro benzaldehyde (100)	75	93	8024	107.2
8	2,4-Dicholorobenzaldehyde oxime	2,4-Dicholorobenzaldehyde (100)	100	96	8301	83.01
9	2,6-Dicholorobenzaldehydeoxime	2,6-Dicholorobenzaldehyde (100)	115	96	8301	69.83
10	3,4-Dimethoxybenzaldehyde oxime	3,4-Dimethoxybenzaldehyde(100)	135	97	8388	79.83
11	3,4,5-Trimethoxybenzaldehyde	3,4,5-Trimethoxybenzaldehyde	140	96	8301	59.29
12	oxime	(100)	180	95	8215	45.63
13	2-Hydroxy benzaldehyde oxime	2-Hydroxy benzaldehyde(100)	135	98	8474	62.77
14	2- Hydroxynaphthaldehydeoxime	2- Hydroxynaphthaldehyde (100)	200	97	8388	41.94
15	Benzophenoneoxime	Benzophenone (100)	160	>99	8561	53.50
16	4- Cholorobenzophenoneoxime	4- Cholorobenzophenone (100)	150	95	8215	54.76
17	Cyclohexanoneoxime	Cyclohexanone (100)	260	96	8301	31.92
18	Cinnamaldehydeoxime	Cinnamaldehyde (100)	160	49	4237	26.48
19	2-Nitro benzaldehyde oxime	2-Nitrobenzonitrile (72)	150	64	5534	36.89
20	4-Nitro benzaldehyde oxime	4- Nitrobenzonitrile (83)	155	53	4583	29.56
	Nicotinaldehydeoxime	3-Nitropridincarboxaldehyde (65)				

[a]Reaction conditions: Oxim, 2 mmol; Cat., 140 mg; Benzaldehyde, 5mmol; tolouene, 6 ml; T = 60 °C; under O_2 bubbling.

[b]TON= Turn Over Number: moles of substrate converted per mole of metal

[c]TOF= Turn Over Frequencies (min^{-1}).

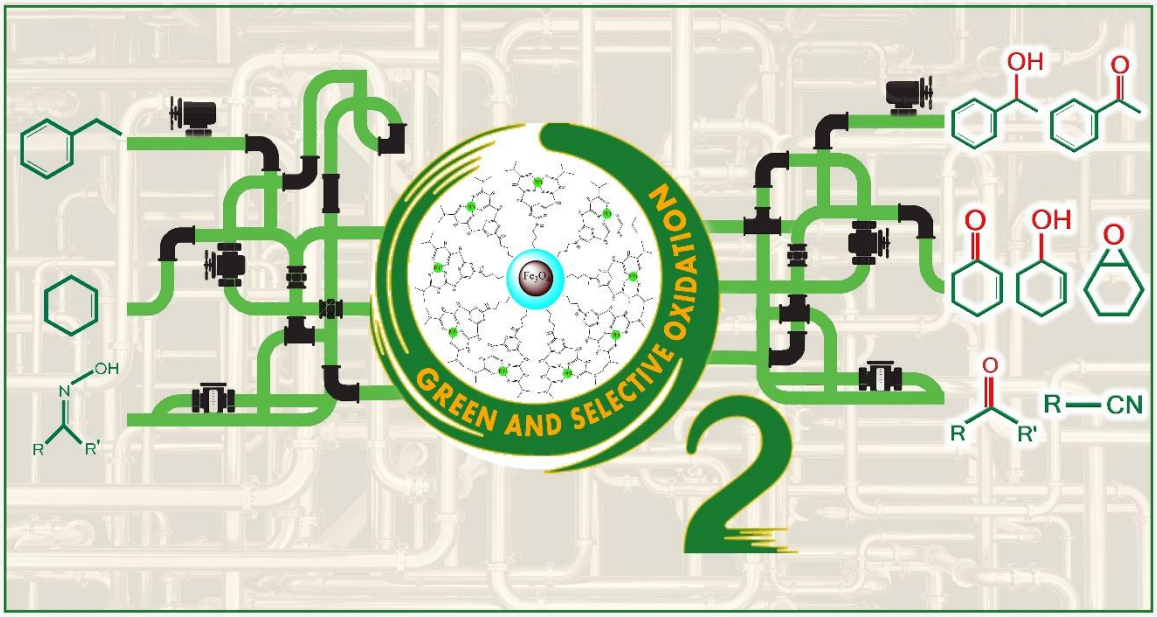

►Supported metformin-manganese complex on modified Fe_3O_4 magnetic nanoparticles was prepared.
►Excellent catalytic activity over transformation of crude and cheap raw materials to usable and chemical industrial materials was observed.
►The nanocatalyst is superior in catalytic activity, selectivity and recyclability in mild conditions and green oxidation process.
►The molecular oxygen was used as an eco-friendly oxidant.